

# Gamma-Ray Burst Precursors as the Remnant of the Thermal Radiation Initially Trapped in the Fireball

Li-Xin Li\*

*Max-Planck-Institut für Astrophysik, 85741 Garching, Germany*

Accepted 2007 June 6. Received 2007 May 31; in original form 2007 March 7

## ABSTRACT

In the standard fireball model of gamma-ray bursts (GRBs), the fireball starts with an optically thick phase. As it expands, the fireball becomes optically thin at some stage. The thermal radiation trapped in the originally opaque fireball then leaks out, producing a transient event. The appearance of the event is investigated in the framework of a homogeneous, spherically symmetric, and freely expanding fireball produced instantly by an explosive process without continuous injection of mass and energy. We find that, generally, the event has a time-duration shorter than that of the main burst, which is presumably produced by the internal shock after the fireball becomes optically thin. The event is separated from the main burst by a quiescent time-interval, and is weaker than the main burst at least in a high energy band. Hence, the event corresponds to a GRB precursor. The precursor event predicted by our model has a smooth and FRED (Fast Rise and Exponential Decay) shape lightcurve, and a quasi-thermal spectrum. Typically, the characteristic blackbody photon energy is in the X-ray band. However, if the distortion of the blackbody spectrum by electron scattering is considered, the characteristic photon energy could be boosted to the gamma-ray band. Our model may explain a class of observed GRB precursors—those having smooth and FRED-shape lightcurves and quasi-thermal spectra.

## Key words:

radiation mechanisms: thermal – relativity – gamma-rays: bursts.

## 1 INTRODUCTION

A standard model for gamma-ray bursts (GRBs) has been the fireball model (Goodman 1986; Paczyński 1986). In this scenario, it is assumed that by whatever a process, a radiation-dominated, optically thick, and baryon-poor plasma fluid is suddenly produced in a compact volume. The radiation field drives the fireball into relativistic expansion, so that a significant fraction of the initial energy of the radiation is converted to the kinetic energy of the fireball (Paczynski 1990; Shemi & Piran 1990). At the end of acceleration, the fireball starts to expand freely with a constant Lorentz factor  $\gtrsim 100$  (Kobayashi, Piran & Sari 1999). Later on, the fireball becomes optically thin and the thermal radiation trapped originally in the fireball starts to leak out. As the fireball becomes sufficiently large, its kinetic energy is converted to the prompt gamma-ray emission through the internal shock and the afterglow emission through the external shock (Rees & Mészáros 1992, 1994; Paczyński & Xu 1994). For a review on the fireball model and the in-

ternal/external shocks, see Mészáros (2006), Piran (1999, 2004), and Zhang & Mészáros (2004).

In many ways a GRB fireball is like a cosmological Big Bang (Peebles 1993). Both theories assume that the event (the GRB and the Universe) starts with a state of a radiation-dominated plasma of very high temperature, in which the production of electron-positron pairs is important, and the plasma is optically thick. The energy of the radiation drives the expansion of the plasma. The plasma and the radiation cool down as the fireball expands. At some moment, the mass density of the plasma becomes low enough so that the plasma becomes optically thin to the photons trapped in it, and the fireball (of the GRB or of the Universe) undergoes a transition from an opaque phase to a transparent phase.

However, a GRB fireball also differs from the Big Bang. The Universe is homogeneous and isotropic at a very high degree. At the time of recombination the fluctuation in the temperature of the cosmic microwave background (CMB) radiation relative to the mean temperature is only  $\sim 10^{-5}$  (Bennett et al. 1996; Smoot et al. 1992). In contrast, the GRB fireball could be highly inhomogeneous and anisotropic. Indeed, the fluctuation in the Lorentz factor of

\* E-mail: lxl@mpa-garching.mpg.de

the fireball is required for the internal shock model to work (Rees & Mészáros 1994; Paczyński & Xu 1994). The Universe is a closed system so that the total energy in it must be conserved. However, the GRB fireball interacts with the surrounding matter and photons are radiated away from its surface. The central engine of the GRB may also continue pumping energy into the fireball even after the prompt GRB emission has ended (Burrows et al. 2007, and references therein). In addition, it is usually assumed that the Universe is infinite, but of course the GRB fireball has a finite volume.

A remarkable success of the Big Bang theory has been the prediction of the existence of a blackbody CMB of temperature  $\approx 3$  K in today's Universe (Gamow 1948a,b; Alpher & Herman 1948) and its detection (Penzias & Wilson 1968; Smoot et al. 1992). The CMB is in fact the cooled remnant of the primeval fireball—an echo of the Big Bang. Because of the expansion of the Universe, the temperature of the CMB is redshifted and is hence very low as the CMB photons reach an observer of today. Similarly, we expect that the GRB fireball has also a remnant of the radiation initially trapped in the fireball, and that the remnant would have a quasi-thermal spectrum. However, because of the fact that the surface of the fireball is assumed to be moving relativistically towards an observer who detects the GRB, the temperature of the radiation as measured by the observer would be significantly boosted by the Doppler effect.

Because of the fact that the radiation in the fireball has a finite energy, the remnant event must have a finite duration. The event starts when the fireball is still optically thick, while the main burst takes place when the fireball is already optically thin. Hence, the remnant event must occur before the main burst, with a smaller distance from the GRB central engine than the main burst. As we will see, the remnant event often has a shorter duration than the main burst (due to the remnant event's smaller distance from the central engine), and is separated from the main burst by a quiescent period of time. Since it is produced by the emission from the photosphere of the fireball, the remnant event should have a spectrum that is dominated by a quasi-thermal component. Hence, at least in a high energy band, the remnant event should look weaker than the main burst. Therefore, the remnant event should be observed as a *precursor* of the GRB.

The aim of the paper is to quantitatively investigate the properties of the GRB precursors as the remnant of the radiation initially trapped in the fireball and look for their possible observational consequences.

In at least several cases, precursors of GRBs have been unambiguously detected. GRB 030406, a burst that was detected out side of the field of view of the International Gamma-Ray Astrophysics Laboratory (*INTEGRAL*), had a precursor that occurred  $\sim 50$  s before the main burst (Marcinkowski et al. 2006). GRB 041219a, a burst that was detected by the *INTEGRAL* Burst Alert System (IBAS), had a precursor that occurred  $\sim 260$  s before the main burst (Vestrand et al. 2005; McBreen et al. 2006). GRB 050820a triggered the Burst Alert Telescope (BAT) onboard *Swift* by a precursor, and Konus/*WIND* by the main burst. The precursor occurred  $\sim 200$  s before the main burst, and the entire duration of the burst is  $\sim 600$  s (Cenko et al. 2006). GRB 060124, also detected by both BAT/*Swift* and

Konus/*WIND*, had a precursor that occurred  $\sim 500$  s before the main burst (Romano et al. 2006). The entire duration is  $\sim 800$  s, making GRB 060124 one of the longest bursts. Another interesting case is GRB 061121, detected by BAT/*Swift* (also by Konus/*WIND* and *RHESSI*), which had a precursor that occurred  $\sim 60$  s before the main burst (Bellm et al. 2006; Fenimore 2006; Golenetskii et al. 2006; Page et al. 2006, 2007).

These observed gamma-ray precursors have the following characters: (1) The precursor is separated from the main burst by a long period of quiescent time; the time separation is comparable to the duration of the main burst. (2) The precursor is weaker than the main burst, and has a shorter time-duration. (3) The precursor often has a smooth and FRED (Fast Rise and Exponential Decay) shape lightcurve. (GRB 050820a is an exception, whose precursor has a lightcurve with at least two peaks.) (4) The precursor has a much softer spectrum than the main burst, and in at least two cases (GRB 030406 and GRB 041219a) the spectrum can be fitted by a blackbody or a blackbody plus a power-law.

On the other hand, Koshut et al. (1995) have found that about 3 percent of the GRBs detected by the Burst and Transient Spectrometer Experiment (BATSE) on the Compton Gamma-Ray Observatory (*CGRO*) have precursors. With a precursor definition different from that of Koshut et al. (1995), Lazzati (2005) has found that about 20 percent of the long-duration BATSE GRBs have evidence of precursor emission.<sup>1</sup> Soft precursor activities in X-rays have been detected in a number of GRBs by *Ginga* (Murakami et al. 1991, 1992) and WATCH onboard *GRANAT* (Sazonov et al. 1998). The precursors detected by *Ginga* have a thermal spectrum with a temperature  $\sim 1$ –2 keV.

On the thermal emission in GRBs, we would also mention that Ryde (2004, 2005) has found that up to 30 percent of long-duration GRBs detected by BATSE/*CGRO* have a spectrum that can be interpreted as combination of a thermal peak plus a power-law component. But his results refer to the prompt gamma-ray emission in the main burst, not the precursor emission.

In this paper, we consider a very simple model for the GRB fireball. By assumption, the fireball is homogeneous and spherically symmetric, and expands with a constant and relativistic speed. The fireball contains a thermal radiation field, but the energy density of the radiation is not large enough to affect the dynamics of the fireball. The rest mass and the kinetic energy of the fireball are conserved. For the radiation field in the fireball, the change in the number of photons is caused only by the emission from the photosphere. Hence, the number of photons is an adiabatically conserved quantity. The last condition requires that the electron-positron pairs have already annihilated. Thus, in addition, we assume that the opacity in the fireball is given by the constant Thompson opacity.

Our model corresponds to the post-acceleration phase of the GRB outflow. This assumption is justified by the fact that the radius of the fireball at the time of photosphere

<sup>1</sup> Lazzati (2005) adopted a definition for a GRB precursor that is in favor of weak precursor emissions and put no limit on the time separation between the precursor and the main burst, hence he found more precursors than Koshut et al. (1995).

emission is much larger than the radius at the end of acceleration (Daigne & Mochkovitch 2002, and Section 5 in the present paper). Our model is similar to that of Goodman (1986) in several aspects: both models assume a freely expanding and optically thick fireball in which an amount of energy was generated instantly at a beginning time, and the observable event is determined by the evolution of the fireball and the radiation in it. There is no continuous injection of energy or mass, unlike the steady wind model of Paczyński (1986, 1990). However, our model also differs from that of Goodman (1986). In the model of Goodman (1986), the fireball is very hot and the process of pair production is very important, and the photosphere was not explicitly included in the calculation. While in our model, the fireball is relatively cool and hence the process of pair production can be ignored (see Section 5 for a justification of this assumption), and the photosphere is calculated in details. In addition, the model of Goodman (1986) [as well as that of Paczyński (1986, 1990)] was aimed to interpret the prompt emission of GRBs (the main bursts), while our model is aimed to interpret the precursor emission of GRBs. This leads to a cooler fireball since a GRB precursor usually has a spectrum that is softer than the main burst.

The paper is organized as follows. In Section 2, we describe the geometry and the kinematics of a GRB fireball, the kinematics of a radiation field in it, and the structure of the photosphere. In Section 3, we describe a formalism for calculating the properties of the precursor event of a GRB arising from the emission by the photosphere, including the luminosity, the blackbody spectrum, and the photon rate observed by a remote observer. In Section 4, we present our numerical results. In Section 5, we derive some scaling relations for the characteristic quantities of the precursor, including the characteristic time scale, the characteristic total energy, and the characteristic photon energy. We also give brief justification for some key assumptions in our model. In Section 6, we discuss the effect of jet collimation, the dependence of our results on the energy band of the detector, and the effect of spectrum distortion by electron scattering. In Section 7, we summarize the results and draw our conclusions.

In Appendix A, we present the simplified results for a limiting case: a photosphere with a constant expansion velocity, which applies to the beginning part of the precursor.

We remark that thermal precursors of GRBs in the internal shock model have been previously studied by Daigne & Mochkovitch (2002). The thermal emission from a GRB photosphere and its effect on the prompt spectrum of a GRB have been investigated by Mészáros & Rees (2000); Mészáros et al. (2002); Ramirez-Ruiz (2005); Rees & Mészáros (2005); Pe'er, Mészáros & Rees (2006); Pe'er et al. (2007); and Thompson, Mészáros & Rees (2007). The emission from a photosphere of a Poynting flux dominated magnetized fireball and its relation to the GRB precursor or the prompt emission of the main burst has been discussed by Lyutikov & Usov (2000); Giannios (2006); and Giannios & Spruit (2007). Our model differs from that adopted in their papers. In their work, they have assumed a steady wind model for the fireball, in which mass and energy are continuously injected into the wind at the center. And, the expansion of the fireball in our model was driven by radiation, not by the Poynting flux as in the magnetic models.

Bianco, Ruffini & Xue (2001) have calculated the thermal emission from a fireball dominated by electron-positron pairs arising from the quantum vacuum polarization process around a charged black hole. The results have been applied to interpretation of the precursor emission, the main burst, as well as the afterglow of GRBs in a unified way (Ruffini et al. 2001, 2002, 2005).

We also remark that thermal precursors produced by the shock wave (or jet) breakout of the progenitor star in the collapsar model of GRBs have been studied by MacFadyen & Woosley (1999); MacFadyen, Woosley & Heger (2001); Ramirez-Ruiz, MacFadyen & Lazzati (2002); and Waxman & Mészáros (2003).

Finally, whenever an observer is referred to in the paper, we ignore the cosmological effect. That is, we assume that the Universe is Euclidean. The correction of the cosmological effect is straightforward, which mainly includes three factors: cosmological redshift to the observed photon energy, time dilation in the observed lightcurve duration, and that the GRB distance appearing in our formulae should be interpreted as the appropriate cosmological distance.

## 2 THE FIREBALL AS A MILNE UNIVERSE

A freely expanding, homogeneous, and spherically symmetric fireball is like a Milne universe (see, e.g., Rindler 1977), except that a fireball has a finite volume but the Milne universe has an infinite volume.

Let us denote the time in the GRB's rest frame by  $t$ , and the spherical coordinates in it by  $\{r, \theta, \phi\}$ . The center of the fireball is at  $r = 0$ . Then, the Minkowski metric is

$$ds^2 = -c^2 dt^2 + dr^2 + r^2 d\Omega^2, \quad (1)$$

where  $d\Omega^2 \equiv d\theta^2 + \sin^2\theta d\phi^2$  is the metric on a two-dimensional sphere of a unit radius.

Define the coordinates  $\eta$  and  $\xi$  by

$$t = \eta \cosh \xi, \quad r = c\eta \sinh \xi, \quad (2)$$

the metric can then be rewritten as the Milne metric

$$ds^2 = -c^2 d\eta^2 + c^2 \eta^2 (d\xi^2 + \sinh^2 \xi d\Omega^2). \quad (3)$$

The trajectory of a particle with a constant radial velocity  $v = \beta c$  is a straight line defined by

$$r = c\beta t, \quad (4)$$

aside from that  $\theta = \text{constant}$  and  $\phi = \text{constant}$ . Equation (4) demonstrates that, at any moment of constant  $t$ , we have  $v \propto r$ . This profile of expansion velocity is typical for explosive events, e.g. supernovae.

By equation (2) we have that, along the trajectory of the particle,

$$\xi = \text{arctanh}\beta, \quad \eta = \gamma^{-1} t, \quad (5)$$

where  $\gamma \equiv (1 - \beta^2)^{-1/2} = \cosh \xi$  is the Lorentz factor of the particle.

Therefore,  $\eta$  represents the proper time of the particle, and  $\xi$  measures the spatial velocity of the particle. The spatial distance in the radial direction on a hypersurface  $\Sigma_\eta$  defined by a constant  $\eta$  is, by equation (3),  $l = c\eta \int_0^\xi d\xi = c\eta\xi$ .

In Fig. 1, we show the spacetime diagram of the fireball.

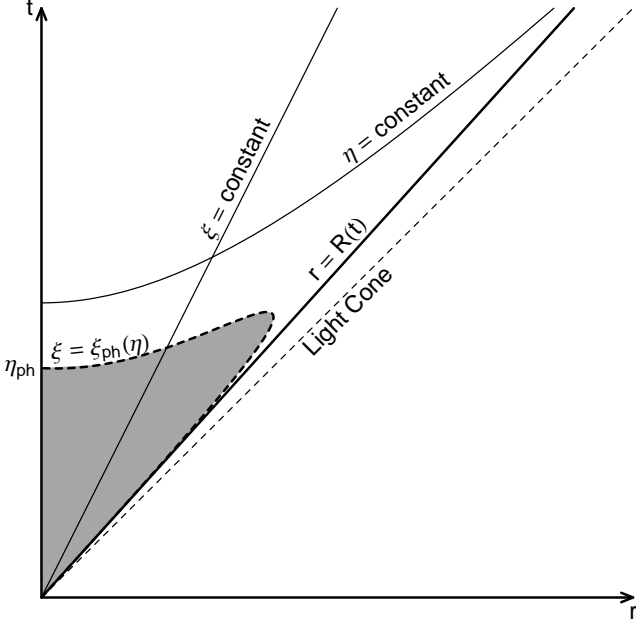


**Figure 1.** The spacetime diagram of a fireball as a Milne universe. Each point represents a two-sphere. The hypersurface  $\xi = \xi_{\text{ph}}(\eta)$  defines the photosphere (Sec. 2.3), within which (the shaded region) the photon optical depth is larger than unity. The photosphere hypersurface becomes spacelike when  $\eta > \eta_0/\sqrt{2}$ , and ends at  $\eta = \eta_{\text{ph}}$ .

The fireball has an outer boundary at  $r = R(t) = c\beta_R t$ , where the expansion velocity is  $v_R = c\beta_R$ , and the Lorentz factor is  $\Gamma = (1 - \beta_R^2)^{-1/2}$ .

## 2.1 The Kinematics of the Fireball

The comoving spatial volume of a sphere of a coordinate radius  $\xi$  on the hypersurface  $\Sigma_\eta$  is

$$V_{\text{com}}(\xi) = 4\pi c^3 \eta^3 \int_0^\xi \sinh^2 \xi d\xi = \pi c^3 \eta^3 (\sinh 2\xi - 2\xi). \quad (6)$$

For a constant  $\xi$ , the comoving volume is  $\propto \eta^3$ .

In the non-relativistic limit  $\beta^2 \approx \xi^2 \ll 1$ , we have  $V_{\text{com}} \approx 4\pi r^3/3$ . In the ultra-relativistic limit  $\gamma = \cosh \xi \gg 1$ , we have

$$V_{\text{com}} \approx 2\pi \gamma^2 c^3 \eta^3 \approx \frac{2\pi}{\gamma} r^3. \quad (7)$$

The fireball has a uniform comoving mass density  $\rho = \rho(\eta) \propto \eta^{-3}$ . The total rest mass contained in the fireball is then

$$M = \rho V_{\text{com}}(\xi_R) = \frac{M_0}{4} (\sinh 2\xi_R - 2\xi_R), \quad (8)$$

where  $\xi_R \equiv \text{arccosh} \Gamma$  is the value of  $\xi$  at the outer boundary of the fireball, and the constant reference mass

$$M_0 \equiv 4\pi \rho \eta^3 c^3. \quad (9)$$

The kinetic energy of the mass contained in a comoving volume element  $dV_{\text{com}}$  bounded by two neighbored spheres of constant radii  $\xi$  and  $\xi + d\xi$  is

$$dE_K = (\gamma - 1)\rho c^2 dV_{\text{com}} = (\cosh \xi - 1)M_0 c^2 \sinh^2 \xi d\xi, \quad (10)$$

which is independent of  $\eta$ . Hence, the total kinetic energy of the fireball is

$$\begin{aligned} E_K &= \int_{\xi=0}^{\xi_R} dE_K \\ &= M_0 c^2 \left( \frac{1}{3} \sinh^3 \xi_R - \frac{1}{4} \sinh 2\xi_R + \frac{1}{2} \xi_R \right). \end{aligned} \quad (11)$$

Equation (11) can also be derived as follows. The stress-energy tensor of the particle fluid is  $T_{ab} = \rho c^2 d\eta_a d\eta_b$ . The energy density measured by a rest observer is  $T_{ab}(\partial/\partial t)^a (\partial/\partial t)^b = \gamma^2 \rho c^2$ . The total energy contained in a hypersurface  $\Sigma_t$  defined by  $t = \text{constant}$  (i.e., a three-space in the rest frame) is thus

$$E = 4\pi \int_0^R \gamma^2 \rho c^2 r^2 dr = \frac{M_0}{c} \int_0^R \gamma^2 \eta^{-3} r^2 dr, \quad (12)$$

where the integral is evaluated on  $\Sigma_t$ . Substituting  $r = c\beta t$  and  $\eta = \gamma^{-1}t$  into equation (12) and treating  $t$  as a constant, we get

$$E = M_0 c^2 \int_0^{\beta_R} \gamma^5 \beta^2 d\beta = \frac{1}{3} M_0 c^2 \sinh^3 \xi_R, \quad (13)$$

where  $\beta = \tanh \xi$  and  $\gamma = \cosh \xi$  have been used. From equations (8) and (13),  $E - Mc^2$  is just the kinetic energy  $E_K$  in equation (11).

When  $\beta_R^2 \ll 1$  ( $\Gamma \approx 1$ , the non-relativistic limit), we have  $M \approx M_0 \beta_R^3/3 \approx 4\pi \rho R^3/3$  and  $E_K \approx M_0 c^2 \beta_R^5/10 \approx 3M v_R^2/10$ . As expected, all these results return to the Newtonian values.

When  $\Gamma = \cosh \xi_R \gg 1$  ( $\beta_R \approx 1$ , the ultra-relativistic limit), we have

$$M \approx \frac{1}{2} M_0 \Gamma^2, \quad (14)$$

and

$$E \approx E_K \approx \frac{2}{3} \Gamma M c^2. \quad (15)$$

In the comoving frame the fireball has a uniform density. However, in the rest frame of the GRB, the density of the fireball increases with radius because of the Lorentz contraction. This effect is particularly important near the outer boundary of the fireball, where the Lorentz factor is dramatically large in the ultra-relativistic case (Fig. 2).

In the rest frame, the number density of the fireball particles is  $\propto \gamma \rho \propto \gamma^4$  on  $\Sigma_t$ . The total energy density is  $\gamma^2 \rho c^2 \propto \gamma^5$ . Hence, in the rest frame both mass and energy are concentrated to a thin spherical shell at the outer boundary. If we consider a thin spherical shell defined by  $R - \Delta R < r < R$  with a thickness (in the rest frame)

$$\Delta R = \frac{R}{2\Gamma^2} \ll R, \quad (16)$$

then by equations (14) and (15), half of the total mass and 64.6 percent of the total kinetic energy are contained in the shell.

## 2.2 The Radiation Field in the Fireball

Assume that the fireball contains a uniform radiation field with a comoving energy density  $e_r$  and a pressure  $p_r = e_r/3$ . From the conservation of energy,  $e_r \propto \eta^{-4}$ . The total energy

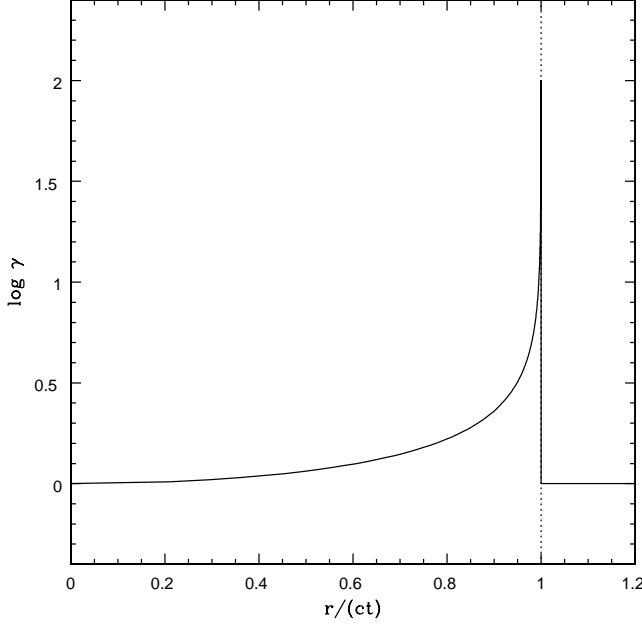


**Figure 2.** The Lorentz factor of particles in the fireball as a function of radius, at any moment of constant  $t$ :  $\gamma = [1 - r^2/(ct)^2]^{-1/2}$ . At the outer boundary of the fireball (the dotted line), the Lorentz factor  $\gamma = \Gamma = 100$ .

of the radiation is not larger than the kinetic energy of the fireball, so that the assumption of a freely expanding fireball is valid ( $\lambda < 1$ , eqs. 24 and 69).

The total energy of the radiation defined in the comoving frame is

$$E_{r,\text{com}} = e_r V_{\text{com}} = \pi e_r c^3 \eta^3 (\sinh 2\xi_R - 2\xi_R). \quad (17)$$

Since  $e_r \propto \eta^{-4}$ , we have  $E_{r,\text{com}} \propto \eta^{-1}$ . As the fireball expands, the total energy of the radiation decreases, caused by the fact that the pressure of the radiation does work. However, since the number density of photons  $n_r \propto \eta^{-3}$ , the total number of photons in the fireball is conserved.<sup>2</sup>

The stress-energy tensor of the radiation field is  $T_{ab} = (e_r + p_r) d\eta_a d\eta_b + (p_r/c^2) g_{ab}$ , where  $g_{ab}$  is the spacetime metric. The energy density in the rest frame is then  $T_{ab} (\partial/\partial t)^a (\partial/\partial t)^b = \gamma^2 e_r + (\gamma^2 - 1) p_r = (4\gamma^2 - 1) e_r/3$ . The total energy of the radiation measured in the rest frame is then

$$E_r = \frac{1}{3} \int_{\Sigma_t} (4\gamma^2 - 1) e_r 4\pi r^2 dr. \quad (18)$$

Using  $e_r \propto \eta^{-4}$ ,  $\eta = \gamma^{-1}t$ , and  $r = c\beta t$ , we get

$$E_r = \frac{4\pi}{3} (e_r \eta^4) c^3 t^{-1} \int_{\Sigma_t} (4\gamma^2 - 1) \gamma^4 \beta^2 d\beta. \quad (19)$$

Since  $\beta = \tanh \xi$  and  $\gamma = \cosh \xi$ , we can work out the integral and obtain

$$E_r = \frac{4\pi}{3} (e_r \eta^4) c^3 t^{-1} \cosh \xi_R \sinh^3 \xi_R. \quad (20)$$

<sup>2</sup> Strictly speaking, the number of photons is an adiabatically conserved quantity since the emission of photons by the photosphere reduces the number of photons in the fireball gradually.

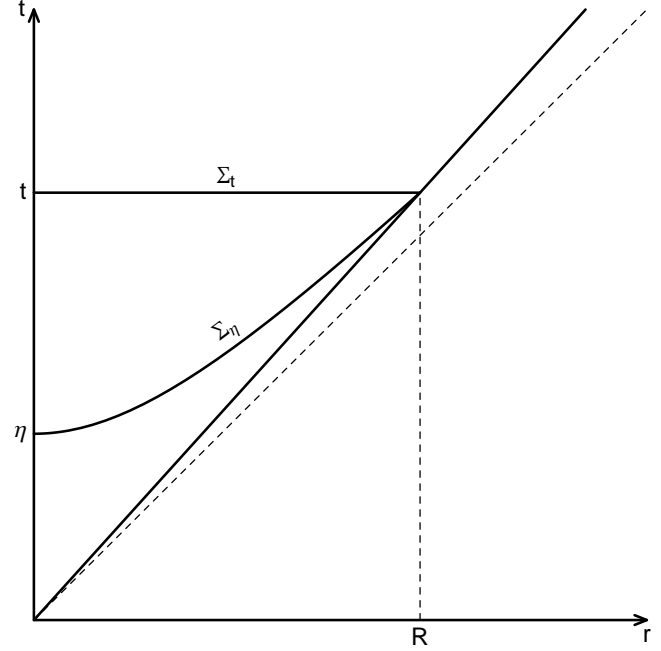


**Figure 3.** The hypersurface on which the total energy of radiation is defined. The energy in the comoving frame,  $E_{r,\text{com}}$ , is defined on  $\Sigma_\eta$  ( $\eta = \text{constant}$ ). The energy in the observer's frame,  $E_r$ , is defined on  $\Sigma_t$  ( $t = \text{constant}$ ).  $\Sigma_t$  and  $\Sigma_\eta$  intersect at  $r = R$  (the outer boundary of the fireball), so that  $E_r$  and  $E_{r,\text{com}}$  are related by equation (21). (The diagonal dashed line represents the light cone.)

Hence,  $E_r \propto t^{-1}$ .

If we define  $\Sigma_\eta$  with the requirement that  $\Sigma_\eta$  intersects  $\Sigma_t$  at  $r = R$  (i.e.,  $\eta = t/\Gamma = t/\cosh \xi_R$ ; see Fig. 3), we can compare the  $E_r$  defined on  $\Sigma_t$  and the  $E_{r,\text{com}}$  defined on  $\Sigma_\eta$ . We have then the effective Lorentz factor of the radiation field

$$\Gamma_{r,\text{eff}} \equiv \frac{E_r}{E_{r,\text{com}}} = \frac{4}{3} \frac{\sinh^3 \xi_R}{\sinh 2\xi_R - 2\xi_R}. \quad (21)$$

When  $\Gamma \approx 1$ , we have  $\Gamma_{r,\text{eff}} \approx 1$ , and  $E_r \approx E_{r,\text{com}} \approx (4\pi/3)e_r R^3$ . When  $\Gamma \gg 1$ , we have  $\Gamma_{r,\text{eff}} \approx 2\Gamma/3$  and

$$E_r|_{\Sigma_t} \approx \frac{2}{3} \Gamma E_{r,\text{com}}|_{\Sigma_\eta} \approx \frac{4\pi}{3} e_r R^3, \quad (22)$$

where  $e_r = e_r(\eta)$  is evaluated on  $\Sigma_\eta$ , and  $R \approx ct$  is the radius of the fireball at time  $t$  (Fig. 3).

At any moment of constant  $t$ , we have  $E_r|_{\Sigma_t} \propto e_r \propto \eta^{-4} \propto \gamma^4$ . Hence, 75 percent of the total radiation energy (defined in the rest frame of the GRB) is contained in the thin shell at the outer boundary of the fireball with a thickness given by equation (16).

We can also compare the total energy of radiation on  $\Sigma_t$  to the total kinetic energy of particles, in the ultra-relativistic limit. By equations (7), (8), and (15), we have

$$E_K \approx \frac{4\pi}{3} \rho R^3 c^2, \quad (23)$$

where  $\rho$  is defined on the  $\Sigma_\eta$  in Fig. 3. Hence, by equation (22), we have

$$\lambda \equiv \frac{E_r}{E_K} \Big|_{\Sigma_t} = \frac{e_r}{\rho c^2} \Big|_{\Sigma_\eta}. \quad (24)$$

To make the model self-consistent, we must require that  $\lambda < 1$ . In our model,  $\rho \propto \eta^{-3}$  but  $e_r \propto \eta^{-4}$ , and so  $\lambda \propto \eta^{-1} \propto t^{-1}$ . Hence, if the condition  $\lambda < 1$  is satisfied at some moment, it will remain being satisfied afterwards. As  $\eta \rightarrow 0$  we have  $e_r/\rho c^2 \rightarrow \infty$  and  $\lambda \rightarrow \infty$ . Hence, there must exist a transition time  $\eta_{\text{acc}}$  defined by  $\lambda(\eta_{\text{acc}}) = 1$ . When  $\eta < \eta_{\text{acc}}$ , the fireball is accelerated by the radiation field. Our model only applies to the free-expansion phase of  $\eta > \eta_{\text{acc}}$ .

### 2.3 The Photosphere of the Fireball

To calculate the photon optical depth in the fireball, we need to consider the geodesics of a photon. Assume that a photon is emitted from a point on a sphere of a comoving coordinate radius  $\xi = \xi_1$  at comoving time  $\eta_1$ , moving outwards in the radial direction. The geodesics of the photon is described by  $r = r_1 + c(t - t_1)$  in terms of  $\{t, r\}$ , where  $t_1$  and  $r_1$  are related to  $\eta_1$  and  $\xi_1$  by equation (2). In terms of  $\{\eta, \xi\}$ , the geodesics can be written as

$$\eta = \eta_1 e^{\xi - \xi_1}. \quad (25)$$

Assume that the opacity in the fireball,  $\kappa$ , is a constant. Then, the optical depth along the trajectory of the photon is (Novikov & Thorne 1973)

$$\tau = \kappa \int \rho dl = \frac{\kappa M_0}{4\pi c^2} \int_{\xi_1}^{\xi_R} \eta^{-2} d\xi, \quad (26)$$

where  $dl = c\eta d\xi$  is radial distance element in the comoving frame, and the integral is along the geodesics of the photon.

Submitting equation (25) into equation (26), we get

$$\tau = \frac{\kappa M_0}{8\pi c^2 \eta_1^2} [1 - e^{-2(\xi_R - \xi_1)}]. \quad (27)$$

When  $\xi_1 = 0$  and  $\beta_R \ll 1$ , we get  $\tau \approx 3\kappa M/4\pi R^2$ , returning to the Newtonian result.

When  $\xi_1 = 0$  and  $\Gamma \gg 1$ , we get

$$\tau \approx \frac{\kappa M_0}{8\pi c^2 \eta_1^2} \approx \frac{\kappa M}{4\pi R_1^2 \Gamma^2}, \quad (28)$$

where  $R_1 \equiv c\eta_1$  is the radius of the fireball at the time when the photon is emitted.

Since  $\tau \propto \eta_1^{-2}$ , at very early time we must have  $\tau \gg 1$  and the fireball must be optically thick. We define the photosphere of the fireball as a hypersurface determined by  $\tau = 1$ . Then, by equation (27), we get the equation for the photosphere

$$\xi_{\text{ph}} = \xi_R + \frac{1}{2} \ln \left( 1 - \frac{\eta^2}{\eta_0^2} \right), \quad (29)$$

where

$$\eta_0 \equiv \left( \frac{\kappa M_0}{8\pi c^2} \right)^{1/2} = \left( \frac{3\kappa E_K}{8\pi c^4 \Gamma^3} \right)^{1/2}. \quad (30)$$

The photosphere hypersurface is shown in Fig. 1. It starts from  $\eta = 0$  as a timelike hypersurface, becomes space-like when  $\eta > \eta_0/\sqrt{2}$  and ends at  $\eta = \eta_{\text{ph}}$ , where

$$\eta_{\text{ph}} \equiv \eta_0 (1 - e^{-2\xi_R})^{1/2}. \quad (31)$$

By the time  $\eta = \eta_{\text{ph}}$ , the radius of the photosphere shrinks to zero. At  $\eta \ll \eta_0$ , we have  $\xi_{\text{ph}} \approx \xi_R$ .

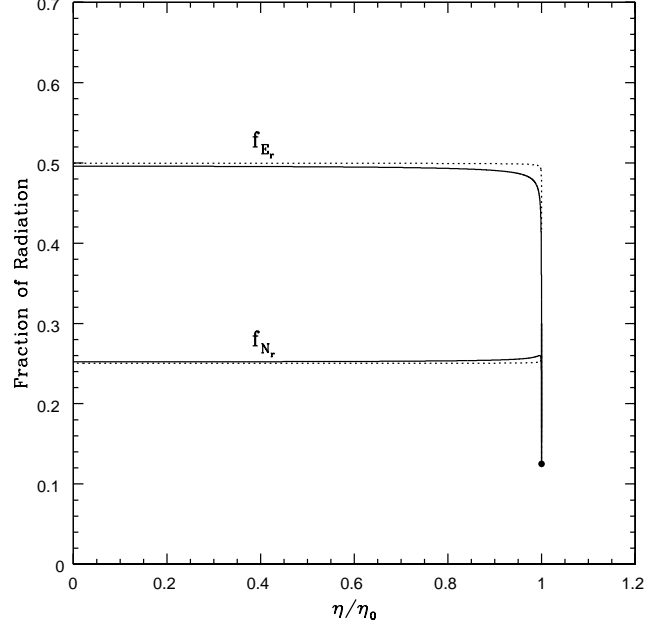


**Figure 4.** The fractions  $f_{E_r}$  (eq. 35, two upper lines) and  $f_{N_r}$  (eq. 36, two lower lines) as functions of  $\eta$ —the comoving time on the photosphere. The solid curves are for  $\Gamma = 100$ . The dotted curves are for  $\Gamma = 1000$ . The maximum of  $\eta$  is  $\eta_{\text{ph}} \approx \eta_0$ , defined by equation (31) and marked by the dot. At  $\eta = \eta_{\text{ph}}$ , we have  $f_{E_r} = f_{N_r} = 1/8$ .

Submitting equation (30) into equation (27), we get

$$\tau = \frac{\eta_0^2}{\eta_1^2} [1 - e^{-2(\xi_R - \xi_1)}]. \quad (32)$$

In the ultra-relativistic limit  $\Gamma = \cosh \xi_R \gg 1$ , we have that  $\eta_{\text{ph}} \approx \eta_0 (1 - 1/8\Gamma^2) \approx \eta_0$ , and  $\tau \approx \eta_0^2/\eta_1^2$  when  $\xi_1 = 0$ .

Although the mass and the energy are concentrated in a thin shell at the outer boundary of the fireball (Sections 2.1 and 2.2), for a photon emitted from the center of the fireball the dominant contribution to the total optical depth comes from the central region. By equation (27) (with  $\xi_1 = 0$  and  $e^{\xi_R} \gg 1$ ), the optical depth is  $\tau/2$  at  $\xi = \ln 2^{1/2} \approx 0.3466$ , where  $\gamma = 3\sqrt{2}/4 \approx 1.0607$ . This is caused by the fact that the mass density decreases quickly as the fireball expands and the optical depth is Lorentz invariant.

For a photon to arrive at the photosphere at a coordinate radius  $\xi_{\text{ph}}$  and comoving time  $\eta$ , the photon must leave the center of the fireball at time  $\eta_1 = \eta e^{-\xi_{\text{ph}}}$ , by equation (25). The photon arrives at a radius  $\xi'$  at time  $\eta' = \eta_1 e^{\xi'} = \eta e^{\xi' - \xi_{\text{ph}}}$ . The total energy of radiation contained in the spheres that have been passed by the photon, evaluated along the geodesics of the photon, is  $\int e_r dV_{\text{com}} \propto \int \eta'^{-1} \sinh^2 \xi' d\xi' \propto \int e^{-\xi'} \sinh^2 \xi' d\xi'$ . The total number of photons contained in the spheres is  $\int n_r dV_{\text{com}} \propto \int \sinh^2 \xi' d\xi'$ .

Let us define

$$\bar{\eta} \equiv \frac{1}{2} (\eta + \eta_1), \quad \bar{\xi} \equiv \ln \left[ \frac{1}{2} (1 + e^{\xi_{\text{ph}}}) \right], \quad (33)$$

on the geodesics of the photon. By equations (29) and (32),

the optical depth at  $\{\bar{\eta}, \bar{\xi}\}$  is

$$\bar{\tau} = \frac{\eta_0^2}{\eta^2} \left(1 - \frac{\eta^2}{\eta_0^2}\right) \left[ \frac{4e^{2\xi_R}}{\left(1 + e^{\xi_R} \sqrt{1 - \eta^2/\eta_0^2}\right)^2} - 1 \right]. \quad (34)$$

The fraction of the energy of radiation contained in the spheres that have been passed by the photon as it arrives at  $\{\bar{\eta}, \bar{\xi}\}$ , to the total energy of radiation contained in the spheres that have been passed by the photon as it arrives at the photosphere, is

$$\begin{aligned} f_{E_r} &= \frac{\int_0^{\bar{\xi}} e^{-\xi'} \sinh^2 \xi' d\xi'}{\int_0^{\xi_{\text{ph}}} e^{-\xi'} \sinh^2 \xi' d\xi'} \\ &= \frac{3e^{\bar{\xi}} + 6e^{-\bar{\xi}} - e^{-3\bar{\xi}} - 8}{3e^{\xi_{\text{ph}}} + 6e^{-\xi_{\text{ph}}} - e^{-3\xi_{\text{ph}}} - 8}. \end{aligned} \quad (35)$$

Similarly, the fraction of the number of photons contained in the spheres that have been passed by the photon as it arrives at  $\{\bar{\eta}, \bar{\xi}\}$ , to the total number of photons contained in the spheres that have been passed by the photon as it arrives at the photosphere, is

$$f_{N_r} = \frac{\int_0^{\bar{\xi}} \sinh^2 \xi' d\xi'}{\int_0^{\xi_{\text{ph}}} \sinh^2 \xi' d\xi'} = \frac{\sinh 2\bar{\xi} - 2\bar{\xi}}{\sinh 2\xi_{\text{ph}} - 2\xi_{\text{ph}}}. \quad (36)$$

In Fig. 4, we plot  $f_{E_r}$  and  $f_{N_r}$  as functions of  $\eta$  on the photosphere. The solid curves are for  $\Gamma = 100$ . The dotted curves are for  $\Gamma = 1000$ . The values of  $1 - f_{E_r}$  and  $1 - f_{N_r}$  give, respectively, the fraction of the total radiation energy and the fraction of the total number of photons contained in the spheres that have been passed by the photon on its last half journey to the photosphere. When  $\eta \lesssim 0.999\eta_{\text{ph}}$ , these fractions are respectively about 50 percent and 75 percent. As  $\eta \rightarrow \eta_{\text{ph}}$ , the fractions approach 87.5 percent.

Inside the photosphere, the radiation has a thermal spectrum with a comoving temperature  $T \propto \eta^{-1}$ . The effective temperature of the radiation emitted by the photosphere, measured in the particle's comoving frame at the photosphere, can be approximated by

$$T_{\text{eff}} = T\bar{\tau}^{-1/4}, \quad (37)$$

where  $T$  is evaluated on the photosphere. Submitting equation (34) into equation (37), and letting  $T = T_0\eta_0/\eta$  where  $T_0$  is the comoving temperature of the radiation at  $\eta = \eta_0$ , we get

$$\begin{aligned} T_{\text{eff}} &= T_0 \left(\frac{\eta}{\eta_0}\right)^{-1/2} \left(1 - \frac{\eta^2}{\eta_0^2}\right)^{-1/4} \\ &\quad \times \left[ \frac{4e^{2\xi_R}}{\left(1 + e^{\xi_R} \sqrt{1 - \eta^2/\eta_0^2}\right)^2} - 1 \right]^{-1/4}. \end{aligned} \quad (38)$$

At  $\eta = \eta_{\text{ph}}$  (where  $\xi_{\text{ph}} = 0$ ), we have  $\bar{\tau} = 1$  and  $T_{\text{eff}} = T_0 [1 - \exp(-2\xi_R)]^{-1/2}$ . When  $\eta \ll \eta_0$ , we have  $\bar{\tau} \approx 3\eta_0^2/\eta^2$  and  $T_{\text{eff}} \approx 3^{-1/4}T_0(\eta/\eta_0)^{-1/2}$ .

### 3 THE QUASI-THERMAL PRECURSOR

In Section 2.3, we have seen that the total optical depth for a photon emitted from the center of the fireball is  $\propto \eta^{-2}$ ,

where  $\eta$  is the comoving time when the photon is emitted (eq. 32). When  $\eta > \eta_{\text{ph}}$ , where  $\eta_{\text{ph}}$  is defined by equation (31), the whole fireball is transparent to photons. When  $\eta < \eta_{\text{ph}}$ , the fireball has a photosphere, within which the plasma is optically thick. The emission from the photosphere has a quasi-thermal spectrum. As we will see, since the emission has a finite amount of energy, it produces a transient event corresponding to the precursor of a GRB.

The photosphere is determined by equation (29). From this section onward, we assume the ultra-relativistic limit  $\Gamma \gg 1$ . Then, we have  $\eta_{\text{ph}} \approx \eta_0$  and  $e^{\xi_R} \approx 2\Gamma$ . Using the coordinates  $\{t, r\}$ , the photosphere hypersurface is determined by the functions of parameter  $\eta$

$$r_{\text{ph}} = \Gamma c\eta \left( \sqrt{1 - \eta^2/\eta_0^2} - \frac{1}{4\Gamma^2 \sqrt{1 - \eta^2/\eta_0^2}} \right), \quad (39)$$

$$t_{\text{ph}} = \Gamma \eta \left( \sqrt{1 - \eta^2/\eta_0^2} + \frac{1}{4\Gamma^2 \sqrt{1 - \eta^2/\eta_0^2}} \right), \quad (40)$$

where  $0 < \eta < \eta_{\text{ph}}$ .

The velocity of a particle on the photosphere is  $\beta_{\text{ph}}c = r_{\text{ph}}/t_{\text{ph}}$ . The Lorentz factor is  $\gamma_{\text{ph}} = t_{\text{ph}}/\eta$ .

The specific flux density of the radiation emitted by the photosphere as measured by a remote observer, whose distance to the fireball is much larger than the radius of the fireball, is

$$F_{E_{\text{obs}}} = \int I_{E_{\text{obs}}} d\Omega_{\text{obs}}, \quad (41)$$

where  $E_{\text{obs}}$  is the observed photon energy,  $I_{E_{\text{obs}}}$  is the observed specific intensity of the radiation, and  $d\Omega_{\text{obs}}$  is the element of the solid angle subtended by the image of the photosphere on the observer's sky.

Because of the fact that  $I_{E_{\text{local}}}/E_{\text{local}}^3$  is invariant along the path of a photon, where  $E_{\text{local}}$  is the energy measured by any local observer on the path (Misner, Thorne & Wheeler 1973), we have  $I_{E_{\text{obs}}} = I_{E_{\text{em}}} E_{\text{obs}}^3/E_{\text{em}}^3$ , where  $E_{\text{em}}$  is the energy of the photon at its point of emission on the photosphere as measured by an observer comoving with the particle emitting the photon, and  $I_{E_{\text{em}}}$  is the specific intensity measured by that observer. Then, equation (41) can be rewritten as

$$F_{E_{\text{obs}}} = \int g^3 I_{E_{\text{em}}} d\Omega_{\text{obs}}, \quad (42)$$

where

$$g \equiv \frac{E_{\text{obs}}}{E_{\text{em}}} = \frac{1}{\gamma_{\text{ph}} (1 - \beta_{\text{ph}} \cos \theta)} \quad (43)$$

is the Doppler factor of the photon, where  $\theta$  is the angle between the photon's wave vector and the velocity of the particle emitting the photon (Jackson 1999).

The local specific intensity of the blackbody radiation emitted by the photosphere has a Planck spectrum

$$I_{E_{\text{em}}} = \frac{1}{h^3 c^2} \frac{2E_{\text{em}}^3}{\exp(E_{\text{em}}/k_B T_{\text{eff}}) - 1}, \quad (44)$$

where  $k_B$  is the Boltzmann constant,  $h$  is the Planck constant, and  $T_{\text{eff}}$  is the effective temperature measured in the comoving frame (eq. 38). Substituting equation (44) into

equation (42), we get

$$F_{E_{\text{obs}}} = \frac{2E_{\text{obs}}^3}{h^3 c^2} \int \frac{d\Omega_{\text{obs}}}{\exp(E_{\text{obs}}/gk_{\text{B}}T_{\text{eff}}) - 1}, \quad (45)$$

where  $E_{\text{em}} = E_{\text{obs}}/g$  has been used.

Without loss of generality, we assume that the observer is located on the polar axis of the fireball ( $\theta = 0$ ), having a distance  $D$  from the center of the fireball. At time  $t_{\text{ph}}$ , a photon is emitted by a particle on the photosphere. The velocity of the particle has an angle  $\theta$  from the polar axis. If the photon is emitted in the direction of the observer, it will arrive at the observer at time

$$t_{\text{obs}} = t_{\text{ph}} - \frac{r_{\text{ph}}}{c} \cos \theta, \quad (46)$$

where we have shifted the origin of the observer's time so that  $t_{\text{obs}} = 0$  if the photon is emitted when the fireball has a zero radius. To arrive at the observer at the same time, photons with different polar angles on the photosphere must be emitted at different time.

In Section 2.3 we have seen that the photosphere hypersurface becomes spacelike when  $\eta > \eta_0/\sqrt{2}$ . That is, after  $\eta = \eta_0/\sqrt{2}$ , the photosphere shrinks superluminally. At  $\eta = \eta_0/\sqrt{2}$ , we have  $\gamma_{\text{ph}} = t_{\text{ph}}/\eta \approx \Gamma/\sqrt{2}$ ,  $r_{\text{ph}} \approx ct_{\text{ph}} = \Gamma c\eta_0/2$ , and  $t_{\text{ph}} - r_{\text{ph}}/c \approx \eta_0/2\Gamma$ . As we will see, because of the relativistic beaming effect, the dominant contribution to the observed radiation comes from a very small region on the photosphere around  $\theta = 0$ . Hence, by equation (46),  $\eta = \eta_0/\sqrt{2}$  corresponds to  $t_{\text{obs}} \approx \eta_0/2\Gamma$ , and

$$t_0 \equiv \Gamma^{-1}\eta_0 = \left(\frac{3\kappa E_{\text{K}}}{8\pi c^4 \Gamma^5}\right)^{1/2} \quad (47)$$

is a critical time parameter of the model.

By equations (39) and (40), equation (46) can be transformed to a cubic equation

$$x^3 - \left(2\mu \sec^2 \frac{\theta}{2}\right) (x^2 + 1) + \left(1 + 4\Gamma^2 \tan^2 \frac{\theta}{2}\right) x = 0, \quad (48)$$

where

$$x \equiv \frac{\eta}{\sqrt{\eta_0^2 - \eta^2}}, \quad \mu \equiv \frac{t_{\text{obs}}}{t_0}. \quad (49)$$

Since  $0 \leq \eta \leq \eta_{\text{ph}}$ , we have  $0 \leq x \leq x_{\text{ph}}$ , where

$$x_{\text{ph}} \equiv \frac{\eta_{\text{ph}}}{\sqrt{\eta_0^2 - \eta_{\text{ph}}^2}} = (e^{2\xi_R} - 1)^{1/2} \approx 2\Gamma. \quad (50)$$

Equation (48), which can be solved analytically, has up to three real roots of  $x$  in the range of  $0 \leq x \leq x_{\text{ph}}$ , depending on the values of  $\theta$ ,  $\mu$ , and  $\Gamma$ . From these roots, we can calculate the corresponding  $\eta$  by the inverse of the first equation in (49). Hence, we can get the comoving time when the photon is emitted from the photosphere

$$\eta_{\text{em}} = \eta_{\text{em}}(\mu, \theta), \quad (51)$$

for a given  $\Gamma \gg 1$ .

The element of the solid angle, after integration over the azimuthal angle  $\phi$ , can be written as a function of  $\theta$  and  $t_{\text{obs}}$

$$d\Omega_{\text{obs}} = \frac{2\pi r_{\text{ph}}^2}{D^2} \sin \theta \cos \theta d\theta. \quad (52)$$

As usual, the azimuthal angle  $\phi$  spans a range of  $0-2\pi$ . However, the polar angle  $\theta$  that contributes to the emissions

received by the remote observer spans only a range of  $0-\theta_{\text{m}}$ , where (Rees 1966; Bianco et al. 2001)

$$\theta_{\text{m}} \equiv \arccos \beta_{\text{ph}} = \arcsin \frac{1}{\gamma_{\text{ph}}} < \frac{\pi}{2}. \quad (53)$$

This is caused by the following fact. Because of the relativistic beaming effect, the radiation emitted by a particle on the photosphere into the hemisphere of a solid angle  $2\pi$  around the normal to the photosphere in the particle's comoving frame, spans only a solid angle  $2\pi(1 - \beta_{\text{ph}})$  around the normal in the rest frame. Photons emitted to the outside of this solid angle will hit the optically thick interior of the photosphere and be absorbed and hence cannot reach the observer (Rees 1966; Bianco et al. 2001).

Then, substituting equation (52) into equation (45), we get

$$F_{E_{\text{obs}}} = \frac{4\pi E_{\text{obs}}^3}{h^3 c^2 D^2} \int_0^{\pi/2} \frac{r_{\text{ph}}^2 \vartheta(\theta_{\text{m}} - \theta) \sin \theta \cos \theta d\theta}{\exp(E_{\text{obs}}/gk_{\text{B}}T_{\text{eff}}) - 1}, \quad (54)$$

where  $\vartheta(\theta_{\text{m}} - \theta)$  is a step function. That is,  $\vartheta(\theta_{\text{m}} - \theta) = 1$  if  $\theta < \theta_{\text{m}}$ ;  $= 0$  otherwise.

After solving for  $\eta_{\text{em}}$  as a function of  $t_{\text{obs}}$  and  $\theta$  (eq. 51), we can evaluate  $r_{\text{ph}}$  and  $t_{\text{ph}}$  (and hence  $\beta_{\text{ph}}$  and  $\gamma_{\text{ph}}$ ) as functions of  $t_{\text{obs}}$  and  $\theta$  by equations (39) and (40),  $g$  by equation (43),  $T_{\text{eff}}$  by equation (38), and  $\theta_{\text{m}}$  by equation (53). Then, the integral in equation (54) can be evaluated.

We remark that, when equation (48) has multiple roots, the contribution of each root to the spectrum integral in equation (54) (as well as to the luminosity and photon rate integrals in eqs. 55 and 56 below) should be summed.

The luminosity as measured by the observer is then

$$\begin{aligned} L &= 4\pi D^2 \int_0^\infty F_{E_{\text{obs}}} dE_{\text{obs}} \\ &= 8\pi \sigma_{\text{SB}} \int_0^{\pi/2} g^4 T_{\text{eff}}^4 r_{\text{ph}}^2 \vartheta(\theta_{\text{m}} - \theta) \sin \theta \cos \theta d\theta, \end{aligned} \quad (55)$$

where  $\sigma_{\text{SB}} = 2\pi^5 k_{\text{B}}^4 / (15h^3 c^2)$  is the Stefan-Boltzmann constant. It can be checked that when the  $r_{\text{ph}}$  and  $T_{\text{eff}}$  are constants and  $g = 1$ , equation (55) gives the standard result for the luminosity of a spherical blackbody.

The lightcurve of a GRB or its precursor is generally not expressed in luminosity. Instead, it is expressed in the photon rate, i.e., the number of photons received by the observer per unit time. By equation (54), the photon rate, which we denote by  $N$ , is

$$\begin{aligned} N &= 4\pi D^2 \int_0^\infty F_{E_{\text{obs}}} d \ln E_{\text{obs}} \\ &= \frac{240\zeta(3)\sigma_{\text{SB}}}{\pi^3 k_{\text{B}}} \\ &\quad \times \int_0^{\pi/2} g^3 T_{\text{eff}}^3 r_{\text{ph}}^2 \vartheta(\theta_{\text{m}} - \theta) \sin \theta \cos \theta d\theta, \end{aligned} \quad (56)$$

where the Riemann zeta function  $\zeta(3) \approx 1.202$ .

## 4 NUMERICAL RESULTS

At very early time when  $\eta^2/\eta_0^2 \ll 1$ , the photosphere expands with a constant velocity that is close to the speed of light, and the formulae for the spectrum, the luminosity, and



the photon rate can be simplified considerably. The results in this limiting case are presented in Appendix A. In fact, the luminosity and the photon rate can be worked out analytically. It turns out that the luminosity  $L$  is a constant, and the photon rate  $N \propto \mu^{1/2}$ , where the dimensionless time  $\mu$  is defined by equation (49).

Although the spectrum cannot be worked out analytically, a remarkable feature of the spectrum is still identified. When  $t_{\text{obs}}$ ,  $E_{\text{obs}}$ , and  $E_{\text{obs}}F_{E_{\text{obs}}}$  are scaled respectively by  $t_0$  (eq. 47),  $E_{\text{ph},0}$  (eq. A5), and  $F_0$  (eq. A8), the spectrum does not depend on the value of  $\Gamma$ , provided that  $\Gamma \gtrsim 100$  (eq. A9). As will be seen in this section, this ‘similarity’ feature persists in the late evolution of the spectrum, the luminosity, and the photon rate up to a time  $\mu \approx 10$ .

From equations (43) and (46), we have  $g = \Gamma\eta/\mu\eta_0$ . Then, using the variables  $\chi$  defined in equation (A5) and  $x$  defined in equation (49), we can write the spectrum integral in equation (54) as

$$\Psi_E = \frac{45}{7\pi^4} \Gamma^2 \chi^4 \int_0^{\pi/2} \frac{x^2 f_1(x) \vartheta(\theta_m - \theta) \sin \theta \cos \theta d\theta}{\exp\left[\mu \chi x^{-1/2} f_2^{1/4}(x)\right] - 1}, \quad (57)$$

where  $\Psi_E \equiv E_{\text{obs}} F_{E_{\text{obs}}} / F_0$  (eq. A8),

$$f_1(x) \equiv \left( \frac{1}{1+x^2} - \frac{1}{4\Gamma^2} \right)^2, \quad (58)$$

and

$$f_2(x) \equiv \frac{1}{3} \left[ \frac{16\Gamma^2}{(1 + 2\Gamma/\sqrt{1+x^2})^2} - 1 \right]. \quad (59)$$

Similarly, for the luminosity and the photon rate, we have

$$\Psi_L = \frac{3\Gamma^2}{7\mu^4} \int_0^{\pi/2} x^4 f_1(x) f_2^{-1}(x) \vartheta(\theta_m - \theta) \sin \theta \cos \theta d\theta, \quad (60)$$

and

$$\Psi_N = \frac{5\Gamma^2}{(8\sqrt{2} - 2)\mu^3} \int_0^{\pi/2} x^{7/2} f_1(x) f_2^{-3/4}(x) \vartheta(\theta_m - \theta) \sin \theta \cos \theta d\theta, \quad (61)$$

where  $\Psi_L \equiv L/L_0$ ,  $L_0$  is the luminosity as  $\mu \rightarrow 0$  (eq. A11); and  $\Psi_N \equiv N/N_0$ ,  $N_0$  is defined by equation (A13).

Equations (57), (60), and (61) have the forms that are convenient for numerical calculations.

First, we calculate the luminosity as a function of  $\mu$  and  $\Gamma$ . The results are shown in Fig. 5, where the solid line is for  $\Gamma = 100$ , and the dashed line is for  $\Gamma = 1000$ . At small  $\mu$ , the solid line is almost identical to the dashed line. Quantitatively, for  $\mu < 10$ , the fractional difference in the two luminosities is  $\lesssim 10$  percent. As  $\mu \rightarrow 0$ , the luminosity  $L$  approaches the constant  $L_0$  (Appendix A). From  $\mu \sim 0.1$ , the luminosity starts to decay with time. At  $\mu = 1$ ,  $L$  drops to  $0.049L_0$ . At very large  $\mu$ , the luminosity depends on the value of  $\Gamma$ .

The luminosity drops to zero as  $\mu$  approaches  $\Gamma$ . This is caused by the following fact. On the photosphere at any comoving time  $\eta$ , the photon emitted by a particle at a larger  $\theta$  reaches the observer at later time. By equation (46), the last photon reaches the observer at  $t_{\text{obs}} = t_{\text{ph}} - r_{\text{ph}} \cos \theta_m / c = t_{\text{ph}} (1 - \beta_{\text{ph}}^2) = \eta / \gamma_{\text{ph}}$ , since photons emitted by particles

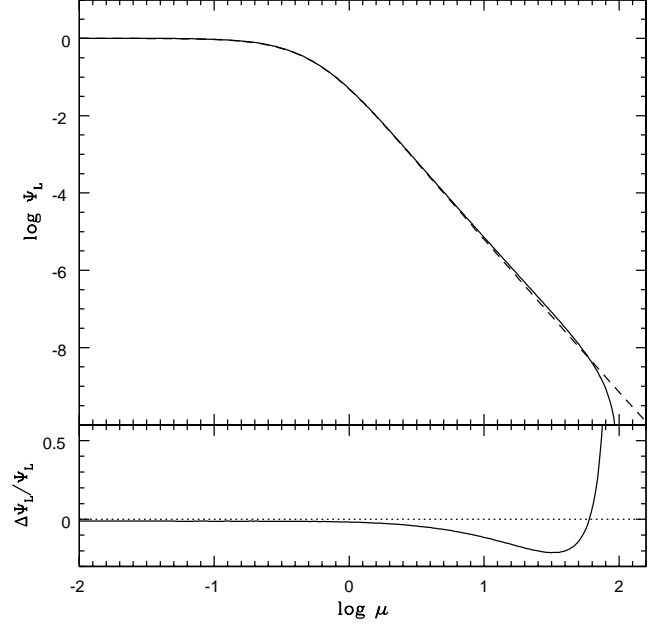


**Figure 5.** Upper panel: the luminosity of the precursor as a function of the observer’s time. The horizontal axis is  $\mu = t_{\text{obs}}/t_0$ . The vertical axis is  $\Psi_L = L/L_0$ . The solid line is for  $\Gamma = 100$ . The dashed line is for  $\Gamma = 1000$ . Lower panel: the fractional difference in the luminosity:  $\Delta\Psi_L/\Psi_L \equiv \Psi_L(\Gamma = 1000)/\Psi_L(\Gamma = 100) - 1$ . The dotted line marks the position of  $\Delta\Psi_L = 0$ .

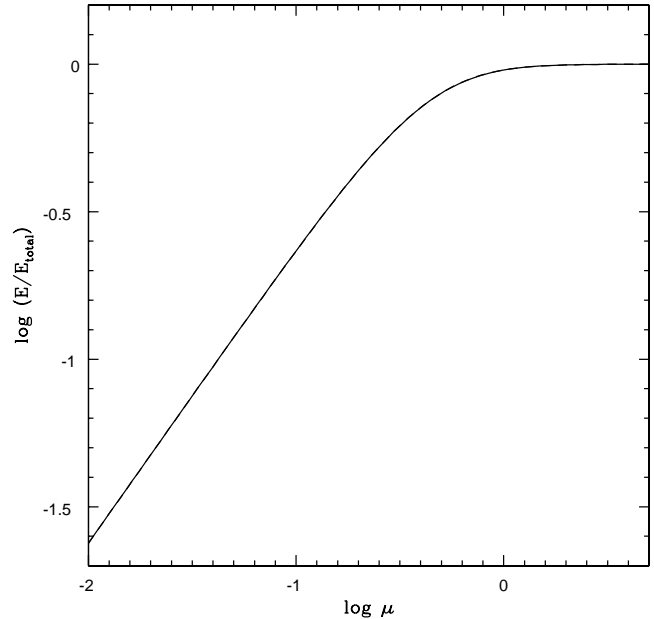


**Figure 6.** The fraction of the accumulated energy in the total energy (eq. 62). The solid line is for  $\Gamma = 100$ . The dashed line is for  $\Gamma = 1000$  (almost indistinguishable from the solid line).

at  $\theta > \theta_m$  are invisible to the observer. Since  $\gamma_{\text{ph}} \geq 1$ , we have  $t_{\text{obs}} \leq \eta \leq \eta_0$ , hence  $\mu = t_{\text{obs}}/t_0 \leq \Gamma$ . That is, the last photon reaches the observer at  $\mu = \Gamma$ .

We can define the accumulated energy of the precursor

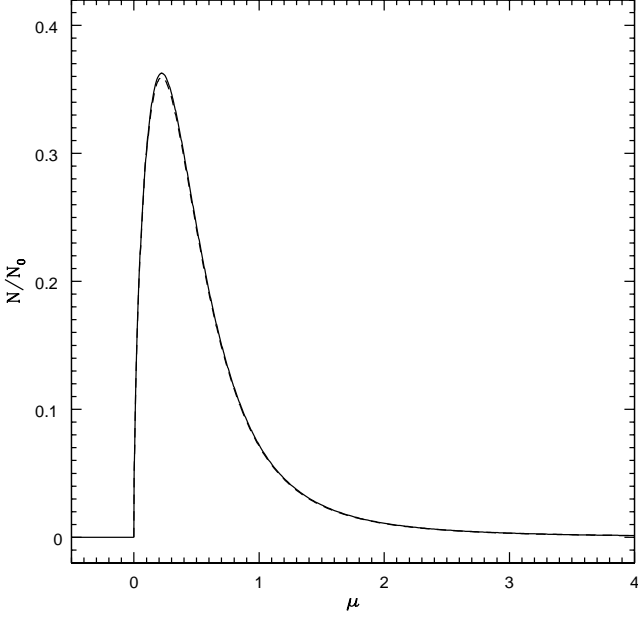


**Figure 7.** The lightcurve of the precursor. The horizontal axis is the observer's time in units of  $t_0$ . The vertical axis is the number of photons per unit time, in units of  $N_0$ . The solid curve is for  $\Gamma = 100$ . The dashed curve is for  $\Gamma = 1000$ .

by

$$E(t_{\text{obs}}) = \int_0^{t_{\text{obs}}} L dt_{\text{obs}} = E_0 \int_0^{\mu} \Psi_L d\mu, \quad (62)$$

where

$$E_0 \equiv L_0 t_0 = \Gamma^{-1} L_0 \eta_0 \quad (63)$$

is a characteristic total energy scale. The total energy emitted by the photosphere is then  $E_{\text{total}} = E(t_{\text{obs}} = \Gamma t_0)$ , which is equal to  $0.426E_0$  when  $\Gamma = 100$ , and  $0.421E_0$  when  $\Gamma = 1000$ .

In Fig. 6 we show the fraction of the accumulated energy in the total energy. At  $\mu = 1$ , about 96 percent of the total energy has been accumulated.

The lightcurve defined by  $\Psi_N = N/N_0$  as a function of  $\mu$  is plotted in Fig. 7, which has a smooth and FRED shape. It starts increasing with time as  $\Psi_N \propto \mu^{1/2}$ , reaches a peak at  $\mu = 0.221$ , then decreases with time quasi-exponentially. The lightcurve has a long tail of soft photons, which lasts until  $\mu = \Gamma$  (see Fig. 5). These soft photons originate from the spacelike part of the photosphere (Fig. 1).

The width of the lightcurve pulse at  $N = N_{\text{max}}/4$  is  $\Delta\mu = 0.895$ . The width at  $N = N_{\text{max}}/20$  is  $\Delta\mu = 1.68$ . The maximum of the photon rate varies slightly with  $\Gamma$ . When  $\Gamma = 100$ , we have  $N_{\text{max}} = 0.363N_0$ . When  $\Gamma = 1000$ , we have  $N_{\text{max}} = 0.359N_0$ . The variation in  $N_{\text{max}}$  is at a level of 1 percent.

The spectra numerically calculated by equation (57) is plotted in Fig. 8, for a sequence of time from  $\mu = 10^{-3}$  to  $\mu = 10^{0.6}$ , with the step in  $\log \mu$  being 0.3. As mentioned above, for the range of time being of interest ( $0 < \mu < 10$ ), the spectrum  $\Psi_E$  is insensitive to the variation of  $\Gamma$ , provided that  $\Gamma \gtrsim 100$ ,  $E_{\text{obs}}$  is scaled by  $E_{\text{ph},0}$ , and  $t_{\text{obs}}$  is scaled by  $t_0$ . In Fig. 8, we plot the spectrum with  $\Gamma = 100$  with solid lines, and the spectrum with  $\Gamma = 1000$  with dashed lines.

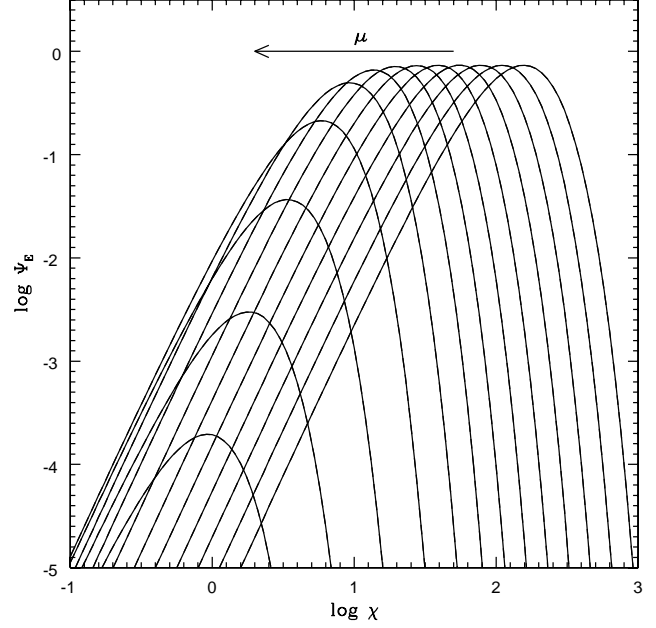


**Figure 8.** The blackbody spectrum of the precursor. The horizontal axis is  $\chi = E_{\text{obs}}/E_{\text{ph},0}$ , which represents the photon energy measured by the observer. The vertical axis is  $\Psi_E = E_{\text{obs}}F_{E_{\text{obs}}}/F_0$ , which represents the energy flux density measured by the observer (see the text for details). Different curves correspond to different observer's time,  $\mu = t_{\text{obs}}/t_0 = 10^{-3}$ – $10^{0.6}$  ( $\Delta \log \mu = 0.3$ ; from right to left as indicated by the arrow). The solid curves are for  $\Gamma = 100$ . The dashed curves (visually indistinguishable from the solid curves) are for  $\Gamma = 1000$ .

As can be seen from the figure, the two results are almost indistinguishable.

A critical parameter characterizing the energy of the photons is the peak spectral energy,  $E_{\text{peak}}$ , which is defined to be the photon energy at the maximum of  $E_{\text{obs}}F_{E_{\text{obs}}}$ . In Fig. 9, we plot  $E_{\text{peak}}$  as a function of time. Since the results are not sensitive to the variation of  $\Gamma$  as we have claimed by Figs. 5–8, in Fig. 9 (similarly in the following figures unless otherwise stated) we show only the plot for  $\Gamma = 100$ . We see that, as  $\mu \rightarrow 0$ ,  $E_{\text{peak}}$  approaches the asymptotic value given by (Appendix A)

$$E_{\text{peak}} = 4.913 E_{\text{ph},0} \mu^{-1/2}. \quad (64)$$

Beyond the maximum of the lightcurve (i.e., when  $\mu > 0.221$ ), the value of  $E_{\text{peak}}$  decays with time faster than that given by equation (64).

In Fig. 10, we show the spectrum at the maximum of the lightcurve ( $\Psi_{E,\text{peak}} = \Psi_E$  at  $\mu = 0.221$ , Fig. 7), and the spectrum integrated over the time interval of  $N/N_{\text{max}} > 1/20$

$$\Psi_{E,\text{int}} = \int_{\mu_1}^{\mu_2} \Psi_E d\mu, \quad (65)$$

where  $\mu_1 = 0.000345$  and  $\mu_2 = 1.68$ . At the low energy end,  $\Psi_{E,\text{int}} \propto \chi^3$ , just as the instant spectrum at any moment. At the high energy end,  $\Psi_{E,\text{int}} \propto \chi^{-2}$ , if we take  $\mu_1 = 0$ .

The integrated spectrum,  $\Psi_{E,\text{int}}$ , peaks at  $\chi = 8.241$ . The spectrum at the maximum of the lightcurve,  $\Psi_{E,\text{peak}}$ , peaks at  $\chi = 10.02$ . Therefore, the peak spectral energy at

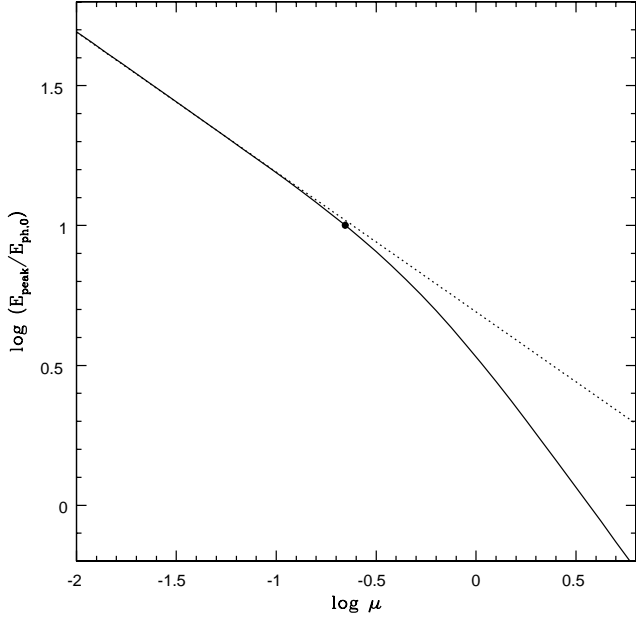


**Figure 9.** The peak energy of the blackbody spectrum as a function of time ( $\Gamma = 100$ ). The point marks the peak energy at the maximum of the lightcurve (at  $\mu = 0.221$ ). The dashed line is the peak energy calculated by equation (64).

the maximum of the lightcurve is

$$E_{\text{peak,max}} = 10.02 E_{\text{ph},0} . \quad (66)$$

The peak spectral energy of the integrated spectrum is

$$E_{\text{peak,int}} = 8.241 E_{\text{ph},0} . \quad (67)$$

## 5 CHARACTERISTIC QUANTITIES

Our model has three characteristic quantities:  $E_{\text{ph},0}$  (eq. A5), a photon energy scale characterizing the peak energy of the spectrum;  $t_0$  (eq. 47), a time scale characterizing the duration and the ‘pulse width’ of the lightcurve; and  $E_0$  (eq. 63), an energy scale characterizing the total energy emitted by the photosphere.

The ratio  $E_0/E_K$  determines the dynamical importance of the radiation field to the fireball. As mentioned in Section 2.2, the importance of the radiation field for the dynamics of the fireball is determined by the parameter  $\lambda$  defined by equation (24), where  $e_r$  is the comoving energy density of the radiation, and  $\rho$  is the comoving mass density of the fireball. Since  $e_r = aT^4 = aT_0^4(\eta/\eta_0)^{-4}$ , where  $T$  is the comoving temperature, and  $a = 4\sigma_{\text{SB}}/c$  is the radiation density constant, by equations (7), (8), and (15) we have

$$\lambda \approx \frac{16\pi\sigma_{\text{SB}}T_0^4\Gamma^3c^2\eta_0^3}{3E_K} \left(\frac{\eta}{\eta_0}\right)^{-1} . \quad (68)$$

By equations (A6), (A11), and (63), we have then

$$\lambda \approx \frac{6L_0\eta_0}{7\Gamma E_K} \left(\frac{\eta}{\eta_0}\right)^{-1} = \frac{6\epsilon_0}{7} \left(\frac{\eta}{\eta_0}\right)^{-1} , \quad (69)$$

where

$$\epsilon_0 \equiv \frac{E_0}{E_K} . \quad (70)$$

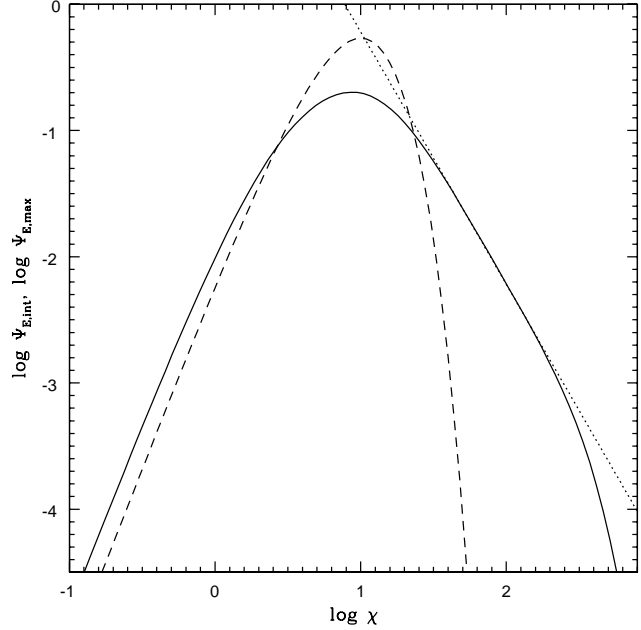


**Figure 10.** The integrated spectrum of the precursor ( $\Psi_{E,\text{int}}$ , integrated over the time interval of  $N/N_{\text{max}} > 1/20$ , eq. 65; solid curve), and the spectrum at the maximum of the lightcurve ( $\Psi_{E,\text{peak}}$ , at  $\mu = 0.221$ ; dashed curve). The dotted line is the asymptotic spectrum at high energy end when the spectrum is integrated from  $\mu = 0$ ,  $\Psi_{E,\text{int}} \propto \chi^{-2}$  (eq. A16).

Hence, at  $\eta = \eta_0$ , we have  $\lambda = 6\epsilon_0/7$ . For the model of a freely expanding fireball to be a good approximation, we must require that  $\epsilon_0 \ll 1$ .

From equations (63), (A5), (A11), and the definitions of  $t_0$  (eq. 47) and  $R_0$  (eq. A6), we can derive that

$$\begin{aligned} E_{\text{ph},0} &= k_B \left( \frac{3E_0}{14\pi ac^3 t_0^3 \Gamma^2} \right)^{1/4} \\ &= 2.073 \text{ keV} \left( \frac{E_0}{10^{52} \text{ erg}} \right)^{1/4} \left( \frac{t_0}{1 \text{ s}} \right)^{-3/4} \\ &\quad \times \left( \frac{\Gamma}{100} \right)^{-1/2} . \end{aligned} \quad (71)$$

If  $E_0$ ,  $E_{\text{ph},0}$ , and  $t_0$  can be measured, then equation (71) can be used to estimate the value of the Lorentz factor  $\Gamma$ .

Since  $\Gamma > 1$ , equation (71) leads to a constraint on  $E_0$ ,  $t_0$ , and  $E_{\text{ph},0}$

$$E_{\text{ph},0} < 20.73 \text{ keV} \left( \frac{E_0}{10^{52} \text{ erg}} \right)^{1/4} \left( \frac{t_0}{1 \text{ s}} \right)^{-3/4} . \quad (72)$$

As we have assumed, the fireball does not contain electron-positron pairs and the opacity in the fireball is dominated by the Thompson electron scattering opacity. Then we have  $\kappa = 0.20(1 + X) \text{ cm}^2 \text{ g}^{-1}$ , where  $X$  is the mass fraction of hydrogen. It is likely that long-duration GRBs arise from the core-collapse of massive stars which have lost their hydrogen envelopes (Woosley & Bloom 2006), hence it is reasonable to assume that  $X = 0$ . Then we have  $\kappa = 0.2 \text{ cm}^2 \text{ g}^{-1}$ .

Then, by equation (47), we have

$$t_0 \approx 1.719 \text{ s} \left( \frac{\kappa}{0.2 \text{ cm}^2 \text{ g}^{-1}} \right)^{1/2} \left( \frac{E_K}{10^{54} \text{ erg}} \right)^{1/2} \times \left( \frac{\Gamma}{100} \right)^{-5/2}. \quad (73)$$

By the definition of  $\epsilon_0$ , equation (70), we have

$$E_0 = 10^{52} \text{ erg} \left( \frac{\epsilon_0}{0.01} \right) \left( \frac{E_K}{10^{54} \text{ erg}} \right). \quad (74)$$

By equations (47), (70), and (71), we have

$$E_{\text{ph},0} \approx 1.381 \text{ keV} \left( \frac{\epsilon_0}{0.01} \right)^{1/4} \left( \frac{\kappa}{0.2 \text{ cm}^2 \text{ g}^{-1}} \right)^{-3/8} \times \left( \frac{E_K}{10^{54} \text{ erg}} \right)^{-1/8} \left( \frac{\Gamma}{100} \right)^{11/8}. \quad (75)$$

By equations (75) and (A5), we have

$$k_B T_0 \approx 0.018 \text{ keV} \left( \frac{\epsilon_0}{0.01} \right)^{1/4} \left( \frac{\kappa}{0.2 \text{ cm}^2 \text{ g}^{-1}} \right)^{-3/8} \times \left( \frac{E_K}{10^{54} \text{ erg}} \right)^{-1/8} \left( \frac{\Gamma}{100} \right)^{3/8}. \quad (76)$$

The very small value of  $k_B T_0$  justifies our assumption that the fireball does not contain pairs.<sup>3</sup>

By equations (47) and (A6), the characteristic radius of the fireball when the thermal precursor emission takes place is

$$R_0 = \Gamma^2 c t_0 \approx 5 \times 10^{14} \text{ cm} \left( \frac{\kappa}{0.2 \text{ cm}^2 \text{ g}^{-1}} \right)^{1/2} \times \left( \frac{E_K}{10^{54} \text{ erg}} \right)^{1/2} \left( \frac{\Gamma}{100} \right)^{-1/2}. \quad (77)$$

The radius of the fireball at the end of acceleration, defined by  $\lambda = 1$  ( $\eta = \eta_{\text{acc}}$ ), is

$$R_{\text{acc}} = \frac{6\epsilon_0}{7} R_0 \approx 4 \times 10^{12} \text{ cm} \left( \frac{\epsilon_0}{0.01} \right) \left( \frac{\kappa}{0.2 \text{ cm}^2 \text{ g}^{-1}} \right)^{1/2} \times \left( \frac{E_K}{10^{54} \text{ erg}} \right)^{1/2} \left( \frac{\Gamma}{100} \right)^{-1/2}. \quad (78)$$

For the model of a freely expanding fireball to be self-consistent, we must require that  $R_{\text{acc}} \ll R_0$ , i.e.  $\epsilon_0 \ll 1$ .

The peak spectral energy is related to  $E_{\text{ph},0}$  by equations (64), (66), and (67). The duration of the precursor (defined by the width of the lightcurve pulse at  $N = N_{\text{max}}/20$ ) is  $\approx 1.7t_0$ . The total energy emitted in the precursor, is  $\approx 0.42E_0$ .

Generally, the characteristic photon energy predicted by our simple model with the assumption of a blackbody photosphere emission is too small for explaining the precursors detected by the gamma-ray detectors, but is in agreement

<sup>3</sup> Even if  $E_{\text{ph},0}$  has a value as high as  $\sim 260$  keV which is likely the case when the blackbody spectrum is distorted by electron scattering (Section 6.3), we have  $k_B T_0 \sim 3$  keV and the effect of pair production is also unimportant at least during the stage when the majority of the precursor photons are emitted.

with the precursors detected by the X-ray detectors (see Introduction; for further discussions see Sec. 6.3).

## 6 DISCUSSIONS

### 6.1 The Effect of Jet Collimation

In our model we have assumed that the fireball is a sphere with a total solid angle of  $4\pi$ . In reality, GRBs are likely to be collimated. That is, the fireball may have a cone shape and spans a solid angle  $\Omega < 4\pi$ . Now we check how this ‘jet collimation’ effect affects our results.

Assume that the fireball spans a solid angle  $\Omega = 4\pi\omega$ ,  $\omega < 1$ . The observer is on the polar axis  $\theta = 0$ , and the polar boundary of the fireball (which is now a cone) is at  $\theta = \theta_c < \pi/2$ , where  $\theta_c \equiv \arccos(1 - 2\omega)$ . In addition, we assume that  $\theta_c \gg \Gamma^{-1}$ , so that the effect of ‘jet collimation’ starts to affect the shape of the lightcurve only at very late time when the Lorentz factor of the photosphere ( $\gamma_{\text{ph}}$ ) drops to a value  $\sim 1/\theta_c$ , just as the observation of the ‘jet break’ signature in GRB afterglow lightcurves (Sari, Piran & Halpern 1999; Friedman & Bloom 2005, and references therein). Hence, we have  $\Gamma^{-2} \ll \omega < 1$ .

With jet collimation, the comoving volume of the fireball in equation (7) should be replaced by

$$V_{\text{com}} \approx 2\pi\omega\Gamma^2 c^3 \eta^3 \propto \omega, \quad (79)$$

where we have let  $\gamma = \Gamma$ . The kinetic energy  $E_K$  is still related to the total mass  $M$  by equation (15), but equation (14) should be replaced by

$$M \approx \frac{\omega}{2} M_0 \Gamma^2, \quad (80)$$

where  $M_0$  is defined by equation (9).

The optical depth is still given by equations (27) and (32), and  $\eta_0$  is still defined by equation (30). Then, for the characteristic time in equation (47), we should replace  $E_K$  by  $E_K/\omega$ . This is equivalent to say that equation (47) still holds if  $E_K$  is interpreted as the isotropic-equivalent kinetic energy.

The photosphere is still defined by equation (29), or equivalently, by equations (39) and (40). The effective temperature of the photosphere is still given by equation (38).

Equation (48) is unchanged, except that  $\theta$  is only allowed to vary in the range of  $0 \leq \theta \leq \theta_c$ .

The specific flux density measured by the observer is still given by equation (54), but the following replacement to the integral over  $\theta$  should be made

$$\int_0^{\pi/2} d\theta \rightarrow \int_0^{\theta_c} d\theta. \quad (81)$$

The luminosity defined by equation (55), after the replacement in equation (81), should be interpreted as the isotropic-equivalent luminosity. The true luminosity of the photosphere should be  $\omega L$ . The same conclusion holds for the photon rate in equation (56).

Because of the relativistic beaming effect, when  $\gamma_{\text{ph}} \gg 1$  the contribution of the photosphere to the observed luminosity, the photon rate, and the spectrum comes from a small region of  $\theta < \gamma_{\text{ph}}^{-1} \ll \theta_c$  on the photosphere. Hence, the effect of the boundary of the jet becomes important only after  $\gamma_{\text{ph}}$  drops to a value smaller than  $\gamma_{\text{ph,br}} \approx \theta_c^{-1}$ . For  $\theta_c \gg \Gamma^{-1}$ ,

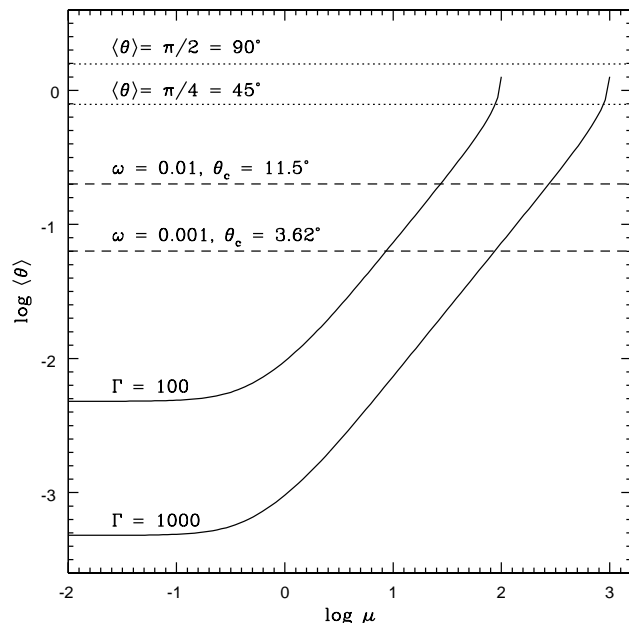


**Figure 11.** The flux-averaged polar angle on the photosphere (solid curves), defined by equation (82). The curve ends at  $\mu = \Gamma$ , since after  $\mu = \Gamma$  no photons emitted by the photosphere can reach the observer. The dashed lines show the maximum polar angle of the cone-shape fireball,  $\theta_c$ . The model of the spherical fireball applies only when the value of  $\langle \theta \rangle$  is below the dashed line (i.e., when  $\langle \theta \rangle < \theta_c$ ). If the photosphere is a static and uniform sphere, we would have  $\langle \theta \rangle = \pi/4$ .

we have  $\gamma_{\text{ph,br}} \ll \Gamma$ , and hence the time  $\mu = \mu_{\text{br}}$  when  $\gamma_{\text{ph}}$  drops to  $\gamma_{\text{ph,br}}$  would be  $\gg 1$ .

We can define a flux-averaged polar angle on the photosphere by

$$\langle \theta \rangle = \frac{8\pi\sigma_{\text{SB}}}{L} \int_0^{\pi/2} \theta g^4 T_{\text{eff}}^4 r_{\text{ph}}^2 \vartheta(\theta_m - \theta) \sin \theta \cos \theta d\theta, \quad (82)$$

for the model of the spherical fireball. If the photosphere is a static and uniform sphere (i.e.,  $g = 1$ ,  $T_{\text{eff}}$  and  $r_{\text{ph}}$  are constants), we would have  $\langle \theta \rangle = \pi/4$ . If the contribution to the luminosity comes from a small region of  $\theta \ll 1$  on the photosphere (which is the case when the photosphere expands relativistically), we would have  $\langle \theta \rangle \ll 1$ . If the contribution to the luminosity comes from a narrow ring region around  $\theta = \theta_0$  on the photosphere, we would expect  $\langle \theta \rangle \approx \theta_0$ .

In Fig. 11, we show the value of  $\langle \theta \rangle$  as a function of time (solid curves). When  $\mu \ll 1$ , the photosphere has a Lorentz factor  $\gamma_{\text{ph}} \approx \Gamma \gg 1$ , the radiation received by the observer comes dominantly from a region of  $\theta \lesssim \Gamma^{-1}$  on the photosphere, hence we have  $\langle \theta \rangle \sim \Gamma^{-1} \ll 1$ . As  $\mu \rightarrow \mu_{\text{max}} = \Gamma$ , the radiation received by the observer comes dominantly from a region of  $\pi/4 < \theta < \pi/2$ .

The dashed lines show the value of  $\theta_c$ , the maximum polar angle of the cone-shape fireball. When  $\langle \theta \rangle \gtrsim \theta_c$ , the observer starts to see the boundary of the cone and the spherical model does not apply any more. As a result, the lightcurve starts to decay faster with time than that predicted by the spherical model. The transition time  $\mu_{\text{tr}}$  (or, the ‘jet break’ time, as commonly called for the GRB afterglow) is approximately determined by  $\langle \theta \rangle = \theta_c$ , i.e. the intersection of the solid curve and the dashed line. When

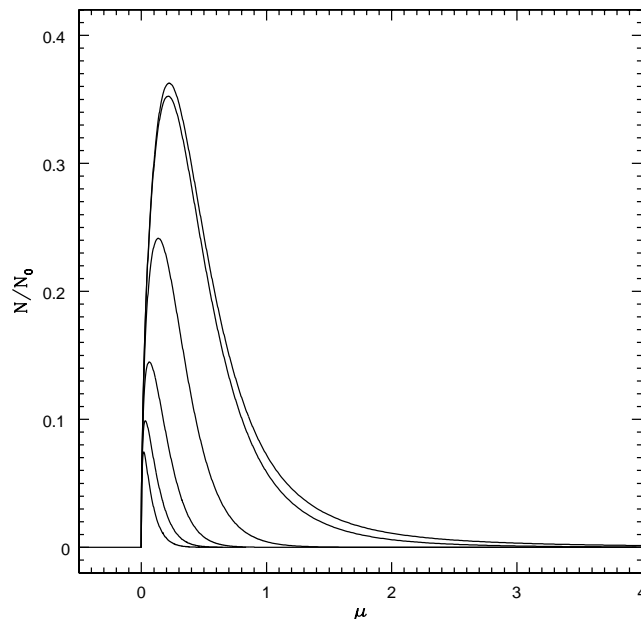


**Figure 12.** The lightcurves detected by detectors with different lower limit on the photon energy. Top to bottom:  $E_{\text{min}}/E_{\text{ph},0} = 0, 1, 5, 10, 15, \text{ and } 20$ .

$\theta_c \gg \Gamma^{-1}$  as we have assumed, the transition time  $\mu_{\text{tr}}$  is much larger than the duration of the event.

Particularly, when  $\mu \ll 1$ , the effect of jet collimation is negligible. The results in Appendix A are unchanged.  $E_{\text{ph},0}$  is still given by equation (A5),  $L_0$  is still given by equation (A11), and  $N_0$  is still given by equation (A13). However, as explained above,  $L_0$  and  $N_0$ , as well as the  $E_{\text{K}}$  in the definition of  $\eta_0$  (eq. 30), should be interpreted as the isotropic-equivalent quantities.

Then,  $E_{\text{ph},0}$  is still the characteristic photon energy, while  $E_0 = L_0 t_0$  is the isotropic-equivalent characteristic total energy. Equations (70)–(77) are then unchanged, if the  $E_{\text{K}}$  and  $E_0$  are interpreted as the isotropic-equivalent kinetic energy and the isotropic-equivalent characteristic total energy, respectively.

## 6.2 Dependence of the Lightcurve and Spectrum on the Energy Band of a Detector

Every detector has a finite range of energy that the detector is sensitive to. For example, the BAT on *Swift* covers an energy range of 15–150 keV, while the BATSE on *CGRO* covers an energy range of 20–1900 keV. The observed lightcurve and the spectrum of a GRB precursor depends crucially on the range of energy of the detector.

We consider only the effect of the lower limit on the photon energy. For a quasi-thermal spectrum the flux density decays quickly at the high energy end, the upper limit on the photon energy is not important provided that it exceeds the peak spectral energy at the maximum of the lightcurve.<sup>4</sup> Hence, we take the lowest energy to be  $E_{\text{min}}$ , and allow the

<sup>4</sup> This could be a problem for *Swift* since the BAT on it has a very small maximum energy.

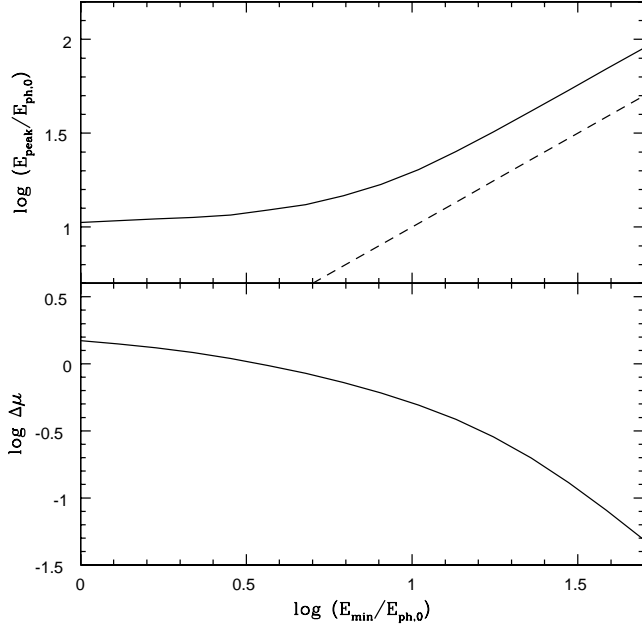


**Figure 13.** The observed peak photon energy of the spectrum at the maximum of the lightcurve (upper panel) and the width of the observed lightcurve pulse (at  $N = N_{\max}/20$ ; lower panel) as functions of the lower energy limit of the detector. The dashed line in the upper panel shows the lower energy limit of the detector.

highest energy to be infinity. Then, the observed photon rate is

$$\Psi_N = \frac{N}{N_0} = \frac{7\pi^4}{36(4\sqrt{2}-1)\zeta(3)} \int_{\chi_{\min}}^{\infty} \chi^{-2} \Psi_E d\chi, \quad (83)$$

where  $\chi_{\min} \equiv E_{\min}/E_{\text{ph},0}$ .

The lightcurves calculated for  $\chi_{\min} = 0, 1, 5, 10, 15,$  and  $20$  are shown in Fig. 12. As  $E_{\min}$  increases, the maximum of the lightcurve shifts to earlier time, and the width of the lightcurve pulse decreases. This is caused by the fact that the energy of the photons emitted by the photosphere decreases with time (Figs. 8 and 9). The maximum photon rate decreases as  $E_{\min}$  increases.

In Fig. 13, we show the observed peak photon energy of the spectrum at the maximum of the lightcurve (estimated by eq. 64) and the width of the observed lightcurve pulse at  $N = N_{\max}/20$  as functions of  $E_{\min}$ . The peak photon energy increases with  $E_{\min}$ , while the width of the lightcurve pulse decreases with  $E_{\min}$ .

### 6.3 Distortion of the Blackbody Spectrum by Electron Scattering

Even if the effects of jet collimation and the finite energy band of the detector are considered, the characteristic photon energy predicted by the model is still significantly smaller than that of the GRB precursors detected by gamma-ray detectors. For example, the spectrum of the precursor of GRB 041219a can be fitted by a blackbody plus a power law. The temperature of the blackbody is  $\approx 46 \pm 9$  keV, corresponding to a peak photon energy  $\approx 180 \pm 35$  keV (in the observer's frame; McBreen et al. 2006). The spectrum of the precursor of GRB 030406 can be fitted by a

blackbody with temperature  $\approx 106 \pm 13$  keV, corresponding to a peak photon energy  $\approx 416 \pm 51$  keV (in the observer's frame; Marcinkowski et al. 2006). However, the peak photon energy of the integrated spectrum predicted by our model is typically  $\approx 8E_{\text{ph},0} \approx 10$  keV, which appears to be consistent with that of the soft X-ray precursors detected by *Ginga* (Murakami et al. 1991, 1992) and WATCH/*GRANAT* (Sazonov et al. 1998).

In our model we have assumed that the emission from the photosphere is a perfect blackbody. However, when electron scattering dominates the opacity, thermal equilibrium exists only when  $\tau_{\text{ff}}\tau_{\text{Th}} > 1$ , where  $\tau_{\text{ff}}$  is the free-free optical depth, and  $\tau_{\text{Th}}$  is the Thompson optical depth (Felten & Rees 1972; Shakura 1972; Shakura & Sunyaev 1973; Novikov & Thorne 1973; Sunyaev & Shakura 1974). At the surface of the fireball, the spectrum of the outgoing radiation is distorted. The energy flux measured in the comoving frame is (Novikov & Thorne 1973)

$$Q = 1.54 \times 10^{-4} n_e^{1/2} T_{\text{eff}}^{9/4} \quad (84)$$

in cgs units, where  $n_e$  is the number density of electrons, and  $T_{\text{eff}}$  is the effective temperature. Equation (84) is in contrast to the standard formula  $Q = \sigma_{\text{SB}} T_{\text{eff}}^4$  for the blackbody.

The characteristic radius for the emission from the photosphere is the  $R_0$  given by equation (77). Let us define the effective temperature of the standard blackbody spectrum in the comoving frame,  $T_{\text{eff},0}$ , by  $L_0 = 4\pi\sigma_{\text{SB}}T_{\text{eff},0}^4R_0^2\Gamma^2$ , where  $L_0$  is related to the characteristic total energy  $E_0$  by equation (63). Similarly, we can define the effective temperature of the distorted blackbody spectrum,  $T_{\text{eff},1}$ , by  $L_0 = 4\pi QR_0^2\Gamma^2$ , where  $Q$  is given by equation (84). Then, we find that

$$\frac{T_{\text{eff},1}}{T_{\text{eff},0}} \approx 23.5 \left(\frac{\epsilon_0}{0.01}\right)^{7/36} \left(\frac{E_{\text{K}}}{10^{54}\text{erg}}\right)^{1/72} \left(\frac{\Gamma}{100}\right)^{-1/24}, \quad (85)$$

where we have assumed that  $\kappa = 0.2 \text{ cm}^2 \text{ g}^{-1}$  and  $n_e = \rho/2m_{\text{H}}$ , where  $m_{\text{H}}$  is the atomic mass unit.

If we take  $E_{\text{peak}} \approx 8E_{\text{ph},0}$ , then equations (75) and (85) imply that

$$E_{\text{peak}} \approx 259 \text{ keV} \left(\frac{\lambda_0}{0.01}\right)^{4/9} \left(\frac{E_{\text{K}}}{10^{54}\text{erg}}\right)^{-1/9} \times \left(\frac{\Gamma}{100}\right)^{4/3}, \quad (86)$$

for the distorted blackbody spectrum. The peak spectral energy given by equation (86), which is defined in the observer's frame, appears to be in agreement with that of the precursors detected by gamma-ray detectors.

Another effect that may help shifting up the photon energy is that the blackbody emission from the photosphere may be nonthermalized by some scattering process and have a nonthermal spectrum. For example, Thompson (1994) has shown that the scattering of the adiabatically cooled thermal photons by the magnetohydrodynamic (MHD) turbulence in the photosphere can boost the thermal photons up to a larger peak energy and lead to a spectrum that have a broken power-law or a Band function (Band et al. 1993) shape.

## 7 SUMMARY AND CONCLUSIONS

We have studied a simple model for the precursor event of a GRB, where the precursor is produced by the emission from the early photosphere of a fireball. The fireball is assumed to be homogeneous, spherical, and expand freely and relativistically. The fireball contains a constant amount of rest mass, and has a constant total kinetic energy. It also contains a radiation field, which drives the acceleration of the fireball expansion at the very early stage, but simply cools down with the expansion at the late free expansion stage. These assumptions make our model different from that has been adopted in the literature for studying the photosphere emission of a GRB, which usually assumes a steady wind with mass and energy injection at the center (Daigne & Mochkovitch 2002; Mészáros & Rees 2000; Mészáros et al. 2002; Ramirez-Ruiz 2005; Rees & Mészáros 2005; Pe'er et al. 2006, 2007; Thompson et al. 2007).

The dynamics of the fireball is the same as that of a Milne universe, except that the fireball has a finite size and contains a finite amount of mass and energy. In the same way as the Universe, at very early time the fireball is opaque to the photons contained in it, but later it becomes transparent (Fig. 1). The photosphere is defined to be the hypersurface where the total optical depth is unity. If the fireball had an infinitely large radius, then as in the Milne universe, the photosphere were just a spacelike hyperbola. However, because of the fact that the fireball has a finite radius, the hypersurface of the photosphere is timelike when  $\eta < \eta_0/\sqrt{2}$ . It is the emission from this timelike part that makes the dominant contribution to the precursor emission detected by a remote observer, since this timelike surface moves towards the observer with a relativistic speed. However, the spacelike part of the photosphere produces a long tail of soft emission.

The luminosity, the photon rate (the lightcurve), and the blackbody spectrum of the precursor are calculated. The results are presented in Figs. 5–10. A remarkable feature of the results is that, when the quantities are properly scaled and the time is not too large, the results are almost invariant with respect to the Lorentz factor of the fireball. That is, if the observer time is in units of  $t_0 = \eta_0/\Gamma$  (eq. 47), the luminosity is in units of  $L_0$  (eq. A11), the photon rate is in units of  $N_0$  (eq. A13), and the spectrum  $E_{\text{obs}}F_{E_{\text{obs}}}$  is in units of  $F_0$  (eq. A8), then the luminosity, the photon rate, and the spectrum are insensitive to the variation of  $\Gamma$  for  $\mu = t_{\text{obs}}/t_0 \lesssim 10$ , provided that  $\Gamma \gtrsim 100$ . At very late time, the results depend on the value of  $\Gamma$ .

Thus, a critical time scale for the precursor is  $t_0$  (eqs. 47 and 73), which is  $\sim 2$  s for typical parameters. The luminosity starts with a constant  $L = L_0$ , and drops to  $L \approx 0.05L_0$  at  $t_{\text{obs}} = t_0$ . The total energy emitted by the photosphere is  $\approx 0.42L_0t_0$ . About 96 percent of the total emitted energy has been accumulated at  $t_{\text{obs}} = t_0$ .

The lightcurve (defined by the photon rate) has a smooth and FRED shape (Fig. 7). It begins as  $N \propto t_{\text{obs}}^{1/2}$ , peaks at  $t_{\text{obs}} \approx 0.22t_0$ , and then decays quasi-exponentially. The width of the lightcurve pulse at  $N = N_{\text{max}}/4$  ( $N_{\text{max}}$  is the maximum photon rate) is  $\Delta t_{\text{obs}} \approx 0.9t_0$ . The width at  $N = N_{\text{max}}/20$  is  $\Delta t_{\text{obs}} \approx 1.7t_0$ .

The blackbody spectrum at different moment of observation is shown in Fig. 8. The peak spectral energy  $E_{\text{peak}}$ , defined to be the photon energy at the maximum of

$E_{\text{obs}}F_{E_{\text{obs}}}$ , decays with time (Fig. 9). Before the maximum of the lightcurve ( $t_{\text{obs}} < 0.22t_0$ ), the peak spectral energy evolves according to, approximately,  $E_{\text{peak}} \propto t_{\text{obs}}^{-1/2}$  (eq. 64). After the maximum, the peak spectral energy decays with time with a rate faster than that given by equation (64) (Fig. 9). At the maximum of the lightcurve ( $t_{\text{obs}} \approx 0.22t_0$ ), the spectrum peaks at  $E_{\text{peak}} = 10.0E_{\text{ph},0}$ , where  $E_{\text{ph},0}$  is the characteristic photon energy defined by equation (A5). The spectrum integrated over the time interval of  $N > N_{\text{max}}/20$  peaks at  $E_{\text{peak}} = 8.24E_{\text{ph},0}$  (Fig. 10).

The characteristic quantities describing the precursor, which include the characteristic time, the characteristic total energy, and the characteristic photon energy are summarized in equations (73)–(75). For typical parameters, the characteristic time is shorter than the duration of a typical long GRB (the main burst), and the characteristic photon energy is in the X-ray band. Because of the thermal nature of the spectrum, at least in the high energy band the total energy is expected to be smaller than the main burst. A constraint on these three characteristic quantities is given by equation (72), which does not depend on the value of the opacity in the fireball.

The characteristic radius of the thermal emission,  $R_0$ , is given by equation (77), which is  $10^{14}$ – $10^{15}$  cm for typical parameters. The internal shock must not occur until the fireball becomes optically thin, since otherwise it would be difficult to explain the nonthermal spectrum of the GRB. Hence,  $R_\delta$ —the radius where the internal shock occurs—must be  $> R_0$ . The time separation between the precursor and the main burst is then  $t_{\text{sep}} \sim R_\delta/2\Gamma^2c$ .

The main burst produced by the internal shock has a duration  $T \approx \Delta/c$ , where  $\Delta$  is the width (measured in the rest frame of the GRB) of the outflow that contributes to the prompt gamma-ray emission (Piran 1999). In our model, the fireball has an expansion velocity  $v \propto r$ , and the majority of mass and energy is confined in a thin layer at the outer boundary of the fireball (Sec. 2.1). The thickness of the layer—which contains 50 percent of total mass and 65 percent of total kinetic energy—is given by equation (16). Letting  $R = R_\delta$ , we have then  $\Delta \approx R_\delta/2\Gamma^2$  and  $T \approx R_\delta/2\Gamma^2c \sim t_{\text{sep}}$ . This relation between the duration of the main burst and the time separation between the main burst and the precursor appears to be consistent with the observation (see Introduction).

We have assumed a spherical fireball. If the GRB outflow is collimated and the resulted fireball has a configuration of a cone spanning a solid angle  $4\pi\omega$  that satisfies  $\Gamma^{-2} \ll \omega < 1$ , the results are still valid until a time is reached when the flux-averaged polar angle of the photosphere increases to a value  $\gtrsim \theta_c = \arccos(1 - 2\omega)$  (Fig. 11). However, in the results,  $L$  and  $N$  should be interpreted as the isotropic-equivalent luminosity and the isotropic-equivalent photon rate respectively. Equations (70)–(77) still hold, but  $E_K$  and  $E_0$  should be interpreted as the isotropic-equivalent kinetic energy and the isotropic-equivalent characteristic total energy of radiation, respectively. This fact is caused by the relativistic beaming effect, which implies that when the photosphere expands relativistically the dominant contribution to the spectrum and the luminosity observed by a remote observer comes from a small region on the photosphere that spans a solid angle  $\sim \Gamma^{-2}$ .

The dependence of the observed lightcurve and spec-

trum on the finite energy range of a detector has also been discussed (Sec. 6.2). Overall, as the lower limit of the detector energy increases, the duration of the lightcurve decreases and the maximum of the lightcurve shifts to earlier time (Figs. 12 and 13). The peak photon energy of the spectrum increases with the lower energy bound of the detector (Fig. 13).

The photon energy predicted by our simple model seems to be consistent with the X-ray precursors of GRBs detected by *Ginga* and WATCH/*GRANAT* (Murakami et al. 1991, 1992; Sazonov et al. 1998), but is too small for the precursors detected by gamma-ray detectors (Cenko et al. 2006; Marcinkowski et al. 2006; McBreen et al. 2006; Romano et al. 2006; Page et al. 2007). However, in our model we have assumed that the emission from the photosphere has a spectrum that is perfectly blackbody. When electron scattering dominates the opacity, the blackbody spectrum is distorted (Felten & Rees 1972; Shakura 1972; Shakura & Sunyaev 1973; Novikov & Thorne 1973; Sunyaev & Shakura 1974). We have estimated this effect by adopting a modified flux equation in equation (84) and found that the distorted spectrum could have a peak spectral energy of  $\sim 260$  keV, which is consistent with the hard spectrum of the observed gamma-ray precursors (Sec. 6.3). Scattering of the soft blackbody photons by e.g. the magnetic turbulence in the fireball may also lead to a nonthermal spectrum (Thompson 1994). A detailed study on these issues is left for our future work.

A strong assumption in our model is that there is no continuous injection of energy and mass, and hence the total mass and the kinetic energy of the fireball are conserved. A big benefit from this simplified assumption is that the shape of the lightcurve and the duration of the emission can be predicted, in contrast to the steady wind model where the lightcurve and the duration depend on the rate of energy and mass injection as a function of time. On the physics side, this type of models with ‘instant release of energy’ may be relevant to the precursors that have smooth and FRED shape lightcurves. More complicated models with continuous injection of mass and energy may be relevant to the precursors that have complex lightcurves.

Although the X-Ray Telescope (XRT) on *Swift* has discovered that flares are common in early X-ray afterglows of GRBs and it seems that the most likely cause of the flares is the late-time activity of the GRB central engine (Burrows et al. 2007, and references therein), the time separation between two adjacent flares are usually much longer than the duration of the precursor event predicted by our model and hence the assumption of no continuous energy and mass injection remains valid. Of course the fireballs or expanding shells related to the late-time activity would also have photosphere emissions. However, the late-time photosphere emissions would overlap with the prompt main GRB emissions or the afterglows (Mészáros & Rees 2000; Mészáros et al. 2002; Ramirez-Ruiz 2005; Rees & Mészáros 2005; Pe’er et al. 2006; Thompson et al. 2007) and hence are hard to detect [see, however, Ryde (2004, 2005); and Pe’er et al. (2007)].

In summary, our model implies the existence of a quasi-thermal precursor of a GRB. The precursor is a remnant of the thermal radiation contained in the fireball during its initial acceleration phase, just like that the CMB is a remnant of the radiation in the Big Bang. The precursor emission has a quasi-thermal spectrum, and a smooth and FRED

shape lightcurve with a duration  $\sim 1\text{--}5$  s. If the distortion of the blackbody spectrum by the electron scattering process is not important, the radiation observed by a remote observer is in the X-ray band with a peak photon energy  $\sim 1\text{--}10$  keV. If the distortion by electron scattering is important, the peak photon energy could be of several hundred keV and hence be in the gamma-ray band. Under some conditions the soft thermal photons may also be nonthermalized and have a nonthermal spectrum. Although in reality the situation may be much more complicated, our simple model may provide a reasonable interpretation for at least a class of GRB precursors—those having smooth and FRED-shape lightcurves and quasi-thermal spectra.

## ACKNOWLEDGMENTS

I am grateful to D. Giannios, F. Meyer, and H. Spruit for helpful conversations on gamma-ray bursts and their precursors, and K. Page, P. Romano, and R. Ruffini for useful communications about their works. I thank the anonymous referee for a very helpful report which has led improvements to the paper.

## REFERENCES

- Alpher R. A., Herman R., 1948, *Nat*, 162, 774  
 Band D. et al., 1993, *ApJ*, 413, 281  
 Bellm E., Bandstra M., Boggs S., Wigger C., Hajdas W., Smith D. M., Hurley K., 2006, *GCN* 5838  
 Bennett C. L. et al., 1996, *ApJ*, 464, L1  
 Bianco C. L., Ruffini R., Xue S.-S., 2001, *A&A*, 368, 377  
 Burrows D. N. et al., 2007, *Phil. Trans. R. Soc. A*, 365, 1213  
 Cenko S. B. et al., 2006, *ApJ*, 652, 490  
 Daigne F., Mochkovitch R., 2002, *MNRAS*, 336, 1271  
 Felten J. E., Rees M. J., 1972, *A&A*, 17, 226  
 Fenimore E. et al., 2006, *GCN* 5831  
 Friedman A. S., Bloom J. S., 2005, *ApJ*, 627, 1  
 Gamow G., 1948a, *Phys. Rev.*, 74, 505  
 Gamow G., 1948b, *Nat*, 162, 680  
 Giannios D., 2006, *A&A*, 457, 763  
 Giannios D., Spruit H. C., 2007, *A&A*, in press (arXiv:astro-ph/0611385v2)  
 Golenetskii S., Aptekar R., Mazets E., Pal’shin V., Frederiks D., Cline T., 2006, *GCN* 5837  
 Goodman J., 1986, *ApJ*, 308, L47.  
 Jackson J. D., 1999, *Classical Electrodynamics*. John Wiley & Sons, New York  
 Kobayashi S., Piran T., Sari R., 1999, *ApJ*, 513, 669  
 Koshut T. M., Kouveliotou C., Paciesas W. S., van Paradijs J., Pendleton G. N., Briggs M. S., Fishman G. J., Meegan C. A., 1995, *ApJ*, 452, 145  
 Lazzati D., 2005, *MNRAS*, 357, 722  
 Lyutikov M., Usov V. V., 2000, *ApJ*, 543, L129  
 MacFadyen A. I., Woosley S. E., 1999, *ApJ*, 524, 262  
 MacFadyen A. I., Woosley S. E., Heger A., 2001, *ApJ*, 550, 410  
 Marcinkowski R., Denis M., Bulik T., Goldoni P., Laurent Ph., Rau A., 2006, *A&A*, 452, 113



McBreen S., Hanlon L., McGlynn S., McBreen B., Foley S., Preece R., von Kienlin A., Williams O. R., 2006, *A&A*, 455, 433

Mészáros P., 2006, *Rept. Prog. Phys.*, 69, 2259

Mészáros P., Rees M. J., 2000, *ApJ*, 530, 292

Mészáros P., Ramirez-Ruiz E., Rees M. J., Zhang B., 2002, *ApJ*, 578, 812

Misner C. W., Thorne K. S., Wheeler J. A., 1973, *Gravitation*. Freeman, San Francisco

Murakami T., Inoue H., Nishimura J., van Paradijs J., Fenimore E. E., 1991, *Nat*, 350, 592

Murakami T., Ogasaka Y., Yoshida A., Fenimore E. E., 1992, in Paciesas W. S., Fishman G. J., eds, *AIP Conference Proceedings*, Vol. 265, *Gamma-Ray Bursts*. Am. Inst. Phys., New York, p. 28

Novikov I. D., Thorne K. S., 1973, in DeWitt C., DeWitt B. S., eds, *Black Holes*. Gordon and Breach, New York, p. 343

Paczynski B., 1986, *ApJ*, 308, L43

Paczynski B., 1990, *ApJ*, 363, 218

Paczynski B., Xu G., 1994, *ApJ*, 427, 708

Page K. L. et al., 2006, *GCN* 5823

Page K. L. et al., 2007, *ApJ*, in press (arXiv:0704.1609v1 [astro-ph])

Peebles P. J. E., 1993, *Principles of Physical Cosmology*. Princeton Univ. Press, Princeton

Pe'er A., Mészáros P., Rees M. J., 2006, *ApJ*, 642, 995

Pe'er A., Ryde F., Wijers R. A. M. J., Mészáros P., Rees M. J., 2007, *ApJ Letters*, submitted (arXiv:astro-ph/0703734v1)

Penzias A. A., Wilson R. W., 1968, *ApJ*, 142, 419

Piran T., 1999, *Phys. Rep.*, 314, 575

Piran T., 2004, *Rev. Mod. Phys.*, 76, 1143

Ramirez-Ruiz E., 2005, *MNRAS*, 363, L61

Ramirez-Ruiz E., MacFadyen A. I., Lazzati D., 2002, *MNRAS*, 331, 197

Rees M. J., 1966, *Nat*, 211, 468

Rees M. J., Mészáros P., 1992, *MNRAS*, 258, 41P

Rees M. J., Mészáros P., 1994, *ApJ*, 430, L93

Rees M. J., Mészáros P., 2005, *ApJ*, 628, 847

Rindler W., 1977, *Essential Relativity: Special, General, and Cosmological*. Springer-Verlag, New York

Romano P. et al., 2006, *A&A*, 456, 917

Ruffini R., Bianco C. L., Frascchetti F., Xue S.-S., Chardonnet P., 2001, *ApJ*, 555, L113

Ruffini R., Bianco C. L., Chardonnet P., Frascchetti F., Xue S.-S., 2002, *ApJ*, 581, L19

Ruffini R., Bernardini M. G., Bianco C. L., Chardonnet P., Frascchetti F., Gurzadyan V., Vitagliano L., Xue S.-S., 2005, in Novello M., Bergliaffa S. E. P., eds, *AIP Conference Proceedings*, Vol. 782, *Cosmology and Gravitation*. Am. Inst. Phys., New York, p. 42

Ryde F., 2004, *ApJ*, 614, 827

Ryde F., 2005, *ApJ*, 625, L95

Sari R., Piran T., Halpern J. P., 1999, *ApJ*, 519, L17

Sazonov S. Y., Sunyaev R. A., Terekhov O. V., Lund N., Brandt S., Castro-Tirado A. J., 1998, *A&AS*, 129, 1

Shakura N. I., 1972, *Sov. Astron.*, 16, 532

Shakura N. I., Sunyaev R. A., 1973, *A&A*, 24, 337

Sunyaev R. A., Shakura N. I., 1974, *Sov. Astron.*, 18, 60

Shemi A., Piran T., 1990, *ApJ*, 365, L55

Smoot G. F. et al., 1992, *ApJ*, 396, L1

Thompson C., 1994, *MNRAS*, 270, 480

Thompson C., Mészáros P., Rees M. J., 2007, *ApJ*, submitted (arXiv:astro-ph/0608282v2)

Vestrand W. T. et al., 2005, *Nat*, 435, 178

Waxman E., Mészáros P., 2003, *ApJ*, 584, 390

Woosley S. E., Bloom J. S., 2006, *ARA&A*, 44, 507

Zhang B., Mészáros P., 2004, *Int. J. Mod. Phys. A*, 19, 2385

## APPENDIX A: PHOTOSPHERE WITH A CONSTANT EXPANSION VELOCITY

When  $\eta^2/\eta_0^2 \ll 1$ , the photosphere defined by equation (29) has a radius  $\xi_{\text{ph}} \approx \xi_R$ , constant  $\gamma_{\text{ph}} = \cosh \xi_{\text{ph}} \approx \Gamma \gg 1$ , and constant  $\theta_m \approx 1/\Gamma \ll 1$ . That is, the photosphere expands with a constant and ultra-relativistic velocity. In this Appendix, we derive the spectrum, the luminosity, and the photon rate of a photosphere in this limiting case.

When  $\eta^2/\eta_0^2 \ll 1$ , we have  $t_{\text{ph}} \approx \Gamma\eta$ ,  $r_{\text{ph}} \approx R \approx \Gamma c\eta$ , and  $\beta_{\text{ph}} \approx \beta_R \approx 1 - 1/2\Gamma^2$ . Then, by equation (43), we have

$$g \approx \frac{1}{\Gamma(1 - \beta_{\text{ph}} \cos \theta)}. \quad (\text{A1})$$

By equations (43) and (46), we have  $t_{\text{obs}} = \eta/g$  and hence

$$\frac{\eta}{\eta_0} = \frac{\mu g}{\Gamma}. \quad (\text{A2})$$

Then, by equations (38) and (A2), we have

$$T_{\text{eff}} \approx 3^{-1/4} T_0 \left( \frac{\eta}{\eta_0} \right)^{-1/2}, \quad (\text{A3})$$

and

$$\frac{E_{\text{obs}}}{g k_B T_{\text{eff}}} \approx \chi \left( \frac{\Gamma \mu}{g} \right)^{1/2}, \quad (\text{A4})$$

where

$$\chi \equiv \frac{E_{\text{obs}}}{E_{\text{ph},0}}, \quad E_{\text{ph},0} \equiv 3^{-1/4} k_B T_0 \Gamma. \quad (\text{A5})$$

Let us define

$$R_0 \equiv \Gamma c \eta_0. \quad (\text{A6})$$

Then,  $r_{\text{ph}}/R_0 \approx \eta/\eta_0 = \mu g/\Gamma$ . By equation (54) we have

$$E_{\text{obs}} F_{E_{\text{obs}}} \approx \frac{10 \sigma_{\text{SB}} T_0^4 R_0^2}{\pi^4 D^2} \Gamma^2 \mu^2 \chi^4 \times \int_0^{\Gamma^{-1}} \frac{g^2 \sin \theta \cos \theta d\theta}{\exp[(\Gamma \mu/g)^{1/2} \chi] - 1}. \quad (\text{A7})$$

Define  $s \equiv g/\Gamma$  and

$$\Psi_E \equiv \frac{E_{\text{obs}} F_{E_{\text{obs}}}}{F_0}, \quad F_0 \equiv \frac{L_0}{4\pi D^2}, \quad (\text{A8})$$

where  $L_0$  is the constant luminosity in the limit  $\eta^2/\eta_0^2 \ll 1$  given by equation (A11) below. By equation (A1), we have  $\cos \theta \approx \beta_{\text{ph}}^{-1} [1 - 1/(\Gamma^2 s)]$  and  $d \cos \theta \approx \beta_{\text{ph}}^{-1} ds/(\Gamma^2 s^2)$ . When  $\theta = 0$ , we have  $s = 2$ . When  $\theta \approx 1/\Gamma$ , we have  $s \approx 1$ . Hence, equation (A7) can be rewritten as

$$\Psi_E \approx \frac{45}{7\pi^4} \mu^2 \chi^4 \int_1^2 \frac{ds}{\exp[(\mu/s)^{1/2} \chi] - 1}. \quad (\text{A9})$$

In equation (A9),  $\chi$  and  $\mu$  appear in the combination  $\mu^{1/2}\chi$ . Hence,  $\Psi_E$  is invariant under the transformation

$$\mu \rightarrow \mu', \quad \chi \rightarrow \chi' = \chi \left( \frac{\mu}{\mu'} \right)^{1/2}. \quad (\text{A10})$$

That is, the value of  $\Psi_E$  at energy  $\chi$  and at time  $\mu$ , is equal to the value of  $\Psi_E$  at energy  $\mu^{1/2}\chi$  and at time  $\mu = 1$ . When  $\mu = 1$ ,  $\Psi_E(\chi)$  peaks at  $\chi = 4.913$ . Hence, at any  $\mu$ ,  $\Psi_E(\chi)$  peaks at  $\chi_{\text{peak}} = 4.913 \mu^{-1/2}$ .

Similarly, for the luminosity in equation (55), we have

$$\begin{aligned} L &\approx \frac{8\pi}{3} \sigma_{\text{SB}} T_0^4 R_0^2 \int_0^{\Gamma^{-1}} g^4 \sin \theta \cos \theta d\theta \\ &\approx L_0 \equiv \frac{56\pi}{9} \sigma_{\text{SB}} T_0^4 R_0^2 \Gamma^2, \end{aligned} \quad (\text{A11})$$

which is a constant.

For the photon rate in equation (56), we have

$$\begin{aligned} N &\approx \frac{80 \cdot 3^{1/4} \zeta(3) \sigma_{\text{SB}}}{\pi^3 k_{\text{B}}} T_0^3 R_0^2 \\ &\quad \times \int_0^{\Gamma^{-1}} g^3 \left( \frac{\eta}{\eta_0} \right)^{1/2} \sin \theta \cos \theta d\theta \\ &= N_0 \mu^{1/2}, \end{aligned} \quad (\text{A12})$$

where

$$\begin{aligned} N_0 &\equiv (4\sqrt{2} - 1) \frac{32 \cdot 3^{1/4} \zeta(3) \sigma_{\text{SB}}}{\pi^3 k_{\text{B}}} T_0^3 R_0^2 \Gamma \\ &= (4\sqrt{2} - 1) \frac{36 \zeta(3)}{7\pi^4} \frac{L_0}{E_{\text{ph},0}}. \end{aligned} \quad (\text{A13})$$

Equations (A11), (A9), and (A12) approximate the numerical results presented in Figs. 7–9 very well for  $\mu \lesssim 0.1$ , with fractional errors  $\lesssim 5$  percent.

The integration of  $\Psi_E$  over  $\mu$  is

$$\int_0^\mu \Psi_E d\mu = \frac{45}{7\pi^4} \chi^{-2} \int_1^2 ds \int_0^{\mu\chi^2} \frac{w^2 dw}{\exp \sqrt{w/s} - 1}, \quad (\text{A14})$$

where  $w \equiv \mu\chi^2$ .

As  $\chi \rightarrow 0$ , we have

$$\int_0^\mu \Psi_E d\mu \approx \frac{12}{7\pi^4} (2^{3/2} - 1) \mu^{5/2} \chi^3 \propto \chi^3. \quad (\text{A15})$$

As  $\chi \rightarrow \infty$ , we have

$$\int_0^\mu \Psi_E d\mu \approx \frac{300\pi^2}{49} \chi^{-2} \propto \chi^{-2}. \quad (\text{A16})$$

This paper has been typeset from a  $\text{\TeX}/\text{\LaTeX}$  file prepared by the author.